Binding Interactions of Ergotamine and Dihydroergotamine to 5-Hydroxytryptamine Receptor 1B (5-HT_{1b}) Using Molecular Dynamics Simulations and Dynamic Network Analysis



Abstract:

Ergotamine (ERG) and dihydroergotamine (DHE), common migraine drugs, have small structural differences, but leading to clinically important distinctions in their pharmacological profiles. For example, DHE is less potent than ERG by about ten-fold at the 5-hydroxytrptamine receptor 1B (5-HT_{1B}). Although the high resolution crystal structures of the 5-HT_{1B} receptor with both ligands have been solved, the high similarity between these two complex structures does not sufficiently explain their activity differences and the activation mechanism of the receptor. Hence, an examination of the dynamic motion of both drugs with the receptor is required. In this study, we ran a total of 6.0 µs molecular dynamics simulations on each system. Our simulation data show the subtle variations between the two systems in terms of the ligandreceptor interactions and receptor secondary structures. More importantly, the ligand and protein root-mean-square fluctuations (RMSF) for the two systems were distinct, with ERG having a trend of lower RMSF values, indicating it to be bound tighter to 5-HT_{1B} with less fluctuations. The Molecular Mechanism-General Born Surface Area (MM-GBSA) binding energies further illustrate this, as ERG has an overall stronger MM-GBSA binding energy. Analysis of several different micro-switches has shown that the 5-HT_{1B}-ERG complex is in a more active conformation state than 5-HT_{1B}-DHE, which is further supported by the dynamic network model, reference to mutagenesis data with the critical nodes and the first three low energy modes from the normal mode analysis. We also identify Trp327^{6.48} and Phe331^{6.52} as key residues involved in the active state 5-HT_{1B} for both ligands. Using the detailed dynamic information from our analysis we made predictions for possible modifications to DHE and ERG that yielded 5 derivatives that might have more favorable binding energies and reduced structural fluctuations.

Abbreviations: 5-HT_{1B}- 5-hydroxytrptamine receptor 1B, BCC, bond charge correction, CWXP, Transmission switch, DHE, dihydroergotamine, DRY, Ionic Lock switch, ERG, ergotamine, GPCR, G Protein-Coupled Receptor, MD, molecular dynamics, MM-GBSA, Molecular Mechanism-General Born Surface Area, NPXXY, Tyrosine Toggle switch, OPLS3, optimized potentials for liquid simulations force field, POPC, phosphatidylcholine, RMSD, rootmean-square deviations, RMSF, root-mean-square fluctuation, r-RESPA, reversible reference system propagation algorithm, SID, simulation interactions diagrams, SPC, simple point charge water model

Introduction:

In designing drug analogs, it has been shown that minor modifications can have significant effects on the action, potency, or selectivity of a drug ¹. This so-called "minor modification rule" illustrates that simple changes such as adding/switching substitutes, hydroxylations, racemate resolutions, isosteric replacements and hydrogenation can greatly change the activities of a drug ¹. In some cases, these simple changes can cause such a difference as to whether a chemical acts as an agonist or antagonist. The imidazolinic compound Efaroxan is an agonist ², but an antagonist when changed to an imidazole ³. Similarly, the benzofuranic compound 2-BFI is an agonist ⁴, but an antagonist when acting as its dihydroderivative ⁵.

Ergotamine (ERG) and its hydrogenated analog, dihydroergotamine (DHE), are another example of this phenomena. ERG is a migraine drug that has been used since 1925 ⁶. It is an alkaloid from the ergot family that has well-documented vasoconstriction effects, one of the main focal points of many migraine drugs ⁷. Due to some persistent common side effects such as nausea, DHE was created in 1945 as an attempt to improve upon the original drug⁸. DHE is structurally similar to ERG, with the only difference being the hydrogenation of a single double bond on ERG's ergoline ring. Interestingly, DHE is a significantly less potent arterioconstrictor than ERG, which makes it a safer drug with less adverse effects such as medication-withdrawal headache, nausea and vomiting ⁹⁻¹¹.

Notably the two drugs have been found to exhibit very different levels of activity at many serotonin and some dopamine receptors. Specifically, seven 5-HT receptor subtypes with various biological activities - 5-HT_{1A}, 5-HT_{1B}, 5-HT_{1D}, and 5-HT_{1F}, 5-HT_{2A}, 5-HT_{2C}, and 5-HT₄ - have been associated with high (but generally very different) affinity for the two ligands ^{7, 12, 13}. Of particular interest in our study is the 5-HT_{1B} receptor, a G-protein-coupled receptor (GCPRs), which has been found to exhibit different activity levels with the ERG and DHE. In the rodent 5-HT_{1B} receptor, ERG was found to display higher activity with a pK_i of 8.69 ¹⁴ compared to

DHE's pK_D of 7.85 15 . Yet despite this significant difference, the drugs' crystal structures show no significant differences (**Figure 1**) and so additional analysis for ligand recognition and selectivity has been impossible 16 .

This study attempts to remedy this by delving deeper into the ligand-protein interactions through molecular dynamics (MD) simulations, which are important tools for understanding the physical basis of the dynamic structure and function of biological macromolecules ¹⁷. MD simulations have been successfully used to probe receptor and ligand dynamics of various GPCR receptors¹⁸⁻²⁵. Though GPCRs have been extensively studied, novel scientific innovations are still on the rise, for example, using MD simulation Yuan and coworkers recently identified a deeper binding pocket that is common to most GPCRs, providing significant opportunities for novel GPCR drug discovery ²⁶ in addition to characterizing the relationship between GPCR activation and internal water pathways²⁷. Li and coworkers used MD simulation to characterize the mechanism of GPCR pituitary adenylate cyclase activating polypeptide (PAC1) shapeshifters ²⁸. Zhang and coworkers published a number of works characterizing the structural diversity of allosteric sites of GPCRs to better understand the drug-target interactions which will ultimately contribute to the design of allosteric drugs with enhanced therapeutic actions ²⁹⁻³¹. Pu and coworkers used MD simulation to elucidate the mechanism driving the allosteric modulation of ligand binding of the C-C chemokine receptor type 5 (CCR5) homodimer³². MD simulation was used by Liu and coworkers to characterize the interactions between high affinity GPCR chemokine receptor 1 (CXCR1) and interleukin-8 ³³. We have also used MD simulation in our previous work to probe the binding of biased agonists to the D2 dopamine receptor ³⁴, the interaction between morphine and IBNtxA in complex with the µ-opioid receptor ³⁵, and described the antagonist activity of fexofenadine to the histamine (H1) receptor³⁶. Specific to the 5-hydroxytryptamine receptor, Sylte et al. ^{37, 38} and Seeber et al. ³⁹ have successfully probed the ligand induced different conformational states of the 5-HT_{1A} receptor using comparative MD

simulations. Another interesting study by Marti-Solano et.al ⁴⁰ showed different dynamic behaviors caused by the binding of ERG to the two subtypes of serotonin receptors (5-HT_{1B} and 5-HT_{2B}) using MD simulations. Their micro-switches analysis has shown that the differences in the conformational freedom of helix 6 between both receptors could explain their different G protein-coupling capacity. In particular, as compared to 5-HT_{1B}, the helix 6 in the 5-HT_{2B} receptor showed a limited movement, blocking the opening of the G protein bonding site and thus reducing G protein coupling ⁴⁰.

Additionally, the use of computational dynamic network models to decipher residueresidue interactions within bimolecular systems and elucidate allosteric communication
pathways have become increasingly popular in recent years. The use of dynamic network models
based on MD trajectories provides an efficient manner to extract correlated motions and
allosteric signals within a complex system that are normally hard to accurately discern by
visualizing MD simulations alone^{41, 42}. From these networks, different regions of the complex
system to be clustered into highly correlated communities which can provide insight into the
effect of ligand binding to the overall communication within the system^{43, 44}. Through use of a
dynamic network model in their work on the μ-Opioid Receptor, Schneider et al. identify the
major residues involved in the induced allosteric communication between the orthosteric binding
pocket and the intracellular region of the receptor⁴⁵. Jiang et al. also used a dynamic network to
elucidate the dynamic and allosteric properties of three GPCR homodimers ⁴⁶. Thus, the use of
dynamic network models have been effectively use to providing experimentally validated insight
into the long-range interactions essential in a variety of allosteric and communication pathways.

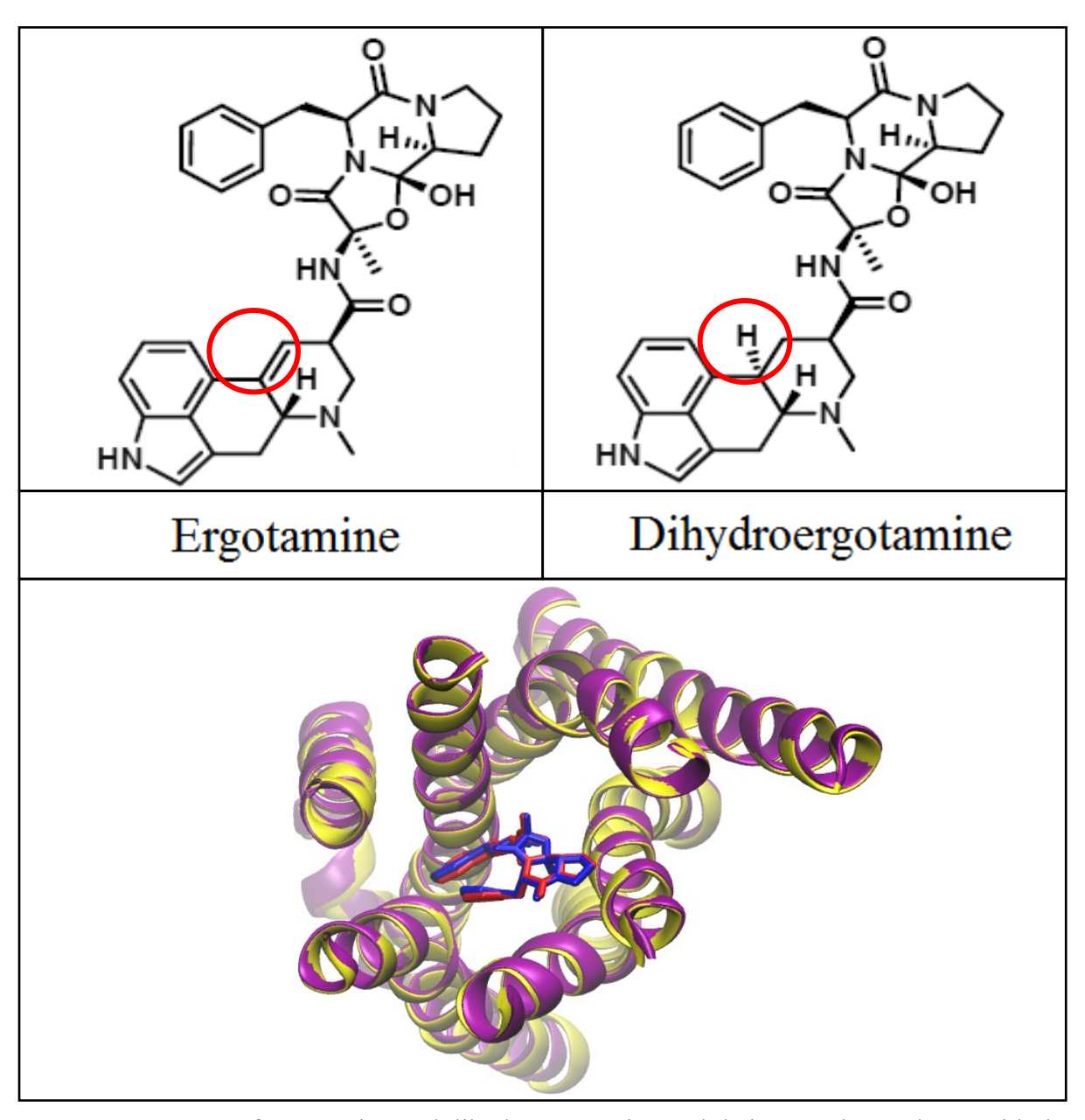


Figure 1 Structure of ergotamine and dihydroergotamine and their crystal complexes with the 5- $\mathrm{HT_{1B}}$ receptor.

In this study, both the ERG- and DHE-5-HT_{1B} complexes from the crystal structures were prepared, processed, and subjected to 6.0 μ s (3x2.0 μ s) molecular dynamics (MD) simulations for each system. The resulting trajectories were combined and compared to find the differences in protein-ligand binding dynamics between the two systems including a dynamic network model. Our data confirmed that DHE, which lacks the additional π bond, is more flexible than

ERG (**Figure 1**). This structural difference causes notable variances in terms of interactions and our analyses highlight the differences in dynamics between the two ligands with the receptor, offering insight as to why the activity of ERG and DHE are so different at the 5-HT_{1B} receptor.

Materials and Methods:

Ligand Preparation. The crystal structures of human 5-HT_{1B} receptor (Figure S1) in complex with DHE (PDB id: 4IAQ) and ERG (PDB id: 4IAR) were downloaded from the Research Collaboratory for Structural Bioinformatics (RCSB) Protein Data Bank. Further preparation of the ligand-protein complex was carried out using Maestro⁴⁷. Initially, the fusion protein and cofactors were removed. The ligand structures were split from the protein and prepared by correcting the bond order and adding the appropriate hydrogens. Calculations of pKa were conducted using Epik, a tool based on accurate methodologies from Hammer and Taft, to get the correct charge state at pH=7.²⁹ The ligands were then merged with the protein to form complexes. These complexes were further preprocessed, optimized, and minimized with the Maestro protein preparation wizard⁴⁷.

Molecular Dynamics Simulation System Setup. The prepared receptor-ligand complexes were then used to construct a molecular dynamics simulation systems. The complex was immersed in a membrane of POPC lipids ⁴⁸ using Maestros system builder and was placed in the predefined position in the membrane using default parameters. Next, it was solvated in an orthorhombic water box with a buffer distance of 10 Å with a SPC water model ⁴⁹. Wang et al. reported POPC lipids are the most favorable option for membrane modeling because they are regularly found in biological membranes and contain an unsaturated carbon-carbon tail, which increases system stabilization ⁵⁰. To neutralize the system, Na⁺ ions were added with a salt concentration of 0.15 M NaCl. The OPLS3 force field was used for modeling the receptor-ligand-lipid system ⁵¹.

MD simulation protocols. Using Desmond module, the system was first relaxed using the default relaxation protocol for membrane proteins ⁵². This relaxation protocol (relax membrane.py) consists of eight steps: 1). Minimization with restraints on solute heavy atoms; 2) Minimization without any restraints; 3). Simulation with heating from 0 K to 300 K, H₂O barrier (i.e. Gaussian Barrier potential on H₂O) and gradual restraining; 4). Simulation under the NPT ensemble (constant number of particles, constant pressure of 1 bar and constant temperature of 300 K) with H₂O barrier and with heavy atoms restrained; 5) Simulation under the NPT ensemble with equilibration of solvent and lipids; 6). Simulation under the NPT ensemble with protein heavy atoms annealing from 10.0 kcal/mol to 2.0 kcal/mol; 7). Simulation under the NPT ensemble with Cα atoms restrained at 2 kcal/mol; and 8). Simulation for 1.5 ns under the NPT ensemble with no restraints. After the relaxation, three 2000.0 ns production runs were conducted under the NPT ensemble for each of the two systems using the default protocol. In details, temperature was controlled using the Nosé-Hoover chain coupling scheme⁵³ with a coupling constant of 1.0 ps. Pressure was controlled using the Martyna-Tuckerman-Klein chain coupling scheme⁵³ with a coupling constant of 2.0 ps. M-SHAKE ⁵⁴ was applied to constrain all bonds connecting hydrogen atoms, enabling a 2.0 fs time step in the simulations. The k-space Gaussian split Ewald method ⁵⁵ was used to treat long-range electrostatic interactions under periodic boundary conditions (charge grid spacing of ~ 1.0 Å, and direct sum tolerance of 10^{-9}). The cutoff distance for short-range non-bonded interactions was 10 Å, and the long-range van der Waals interactions was based on a uniform density approximation. To reduce the computation, non-bonded forces were calculated using an r-RESPA integrator⁵⁶ where the short range forces were updated every step and the long range forces were updated every three steps. The trajectories were saved at 50.0 ps intervals for analysis. The three independent simulations per system were combined for analysis.

Convergence of Simulation. To check the convergence of MD simulations, we investigated the average protein Cα and ligand RMSD plots for both trajectories (Figure S2). The plots depict relatively flat changes within the last 900 ns, providing evidence that the system had reached a steady state.

Trajectory Clustering Analysis. Complex structures from the last 500 ns of the two simulations of each ligand-protein system were grouped to find top structural families with abundance for each ligand. The Desmond trajectory clustering tool ⁵⁷, with Backbone RMSD matrix as the structural similarity matrix, hierarchical clustering with average linkage for the clustering method, and a merging distance cutoff set at 2.5 Å, was used for this analysis ⁵⁷. The structure with the greatest number of neighbors in the structural family, called the centroid structure, was used for representation (**Figure 2**). All clusters are shown in **Figure S3**.

Simulation interaction diagram (SID) analysis. The Desmond SID tool was used to analyze the receptor-ligand interactions throughout the MD trajectory. Particular attention was given to ligand-residue interactions (Figure 3-4), secondary structure changes (Figure 5), protein Cα Root Mean Square Fluctuation/RMSF (Figure 6), ligand RMSF (Figure 7), and ligand torsion plots (Figure 8). In addition to this, we use our simulation data to analyze a number of molecular switches (Figure 9; Figure S8-S9). In reference to these figures we define antagonist as a molecule whose binding results in the receptor being in an inactive state and an agonist as a molecule that activates the receptor when bound. In addition we reference the active and inactive states of these molecular switches, which refer to the position of the transmembrane helix involved in the molecular switch when bound to an antagonist (inactive conformation) and agonist (active conformation) and comparisons are made from the crystal structure.

Binding energy Calculations and decomposition methods. Molecular Mechanism-General Born Surface Area (MM-GBSA) binding energies were calculated on the 2x50 frames in the last 500ns for both systems (**Table 1**). Prior studies found MM-GBSA to be useful when ranking and

comparing ligands ⁵⁸⁻⁶⁰. The surface-area-based Generalized Born model ^{61,62} with implicit membrane model was used (VSGB 2.0) in the calculation. The implicit membrane is a slabshaped region with a low dielectric constant between 1 and 4, and the regions to exclude from membrane is assigned with the solvent (water) dielectric constant of 80. The OPLS3 force field and the default Prime protocol was used. The OPLS3 force field employs a CM1A-BCC based charge model based on a combination of Cramer-Truhlar CM1A charges ⁵¹ with an extensive parameterization of bond charge correction terms (BCC). The default procedure consists of three steps: Receptor alone, Ligand alone, Receptor-ligand complex. The original interaction terms include Coulombic, H-bond, GB solvation, van der Waals, pi-pi packing, self-contact, and lipophilic. The total binding free energy equation was then done: $\Delta E_{\text{(bind)}} = E_{\text{complex}} - E_{\text{ligand}} +$ $E_{receptor}$. The interaction terms were then merged into three components, $E_{electrostatics}$, E_{vdW} , and Elipophilic, for increased understanding of binding nature: where Eelectrostatics = H_{bond} + E_{coulomb} $+E_{GB \text{ solvation}}$, $E_{vdW} = E_{vdW} + E_{\pi-\pi} + E_{self\text{-contact}}$ and $E_{lipophilic}$. The MM-GBSA scoring function lacks the solute conformational entropy which results in higher negative values when compared to the actual values. Nevertheless, when used to rank different drugs targeting receptors with comparable binding entropy values, it has proven to be extremely useful ⁵¹. Previous works, including the use of 1,864 crystal complexes, have shown that MM-GBSA is a powerful tool in ranking ligands ^{58-60, 63, 64}. Further evaluation of the binding energy calculations were performed by decomposing the MM-GBSA data by residue and comparing those more favorable than -2.0 kcal/mol (Table 2).

Dynamical Network Model

The combined trajectories of each system were used to generate a dynamic network model, defined as a set of nodes connected by edges, ^{45, 65-68} using the NetworkView plugin^{65, 69} in VMD ⁷⁰. For each system, we generated a contact map which added an edge between nodes whose heavy atoms interacted within a cutoff of 4.5Å for at least 75% of the MD simulation time. The 4.5Å distance

cutoff was explicitly chosen based on the work of Luthey-Schulten and coworkers⁶⁹ where they studied distance cut offs ranging from 3.5-5.0Å and found the data from the 4.5Å cut off showed the least difference community repartition, therefore showed the least change in the community distributions of the network. In this contact map, the edge distance was derived from pairwise position fluctuation correlations⁶⁵ using the program Carma⁷¹, (**Figure 10**) which defines the probability of information transfer across a given edge using the following equation:

$$C_{ij} = \frac{\langle \vec{\Delta r_i}(t) \cdot \vec{\Delta r_j}(t) \rangle}{(\langle \vec{\Delta r_i}(t)^2 \rangle \langle \vec{\Delta r_j}(t)^2 \rangle)^{1/2}}$$

Using the pairwise correlation data in the dynamic network model, the edges are weighted (w_{ij}) between two nodes i and j using the following calculation^{65, 69}: $w_{ij} = -\log(|C_{ij}|)$. This method of weighting is based on the correlated motion in the simulation trajectory whereby the weight of the edge represents the probability for information to transfer across the edge between the two nodes, thus, a thicker edge represents a lower probability of information transfer. In addition to weighting networks based on the correlated motion in the simulation trajectory, the networks may also be weighted based on the strength on interactions within a single structure as demonstrated by Bhattacharyya, Bhat, and Vishveshwara⁷² as well as Gadiyarum, Vishveshwara, and Vishveshwara⁷³.

Each network was then further grouped into subnetworks, termed communities, based on groups of nodes with stronger and more frequent connection to each other. This was done by applying the Girvan-Newman algorithm to the original network⁷⁴. Critical nodes that connect communities to another were also identified (**Figure 10**). Using the molecular switch data, an optimal communication path was generated between the ligand node and the molecular switch residue (**Figure 11**).

Normal Mode Analysis

The combined trajectories for each system were used in the VMD Normal Mode Wizard 75 to

generate a principal component analysis of the top 10 normal modes (Figure S10).

Virtual Screening

Two and three derivatives were chosen from a virtual screening of ergotamine and dihydroergotamine derivative libraries, respectively, using Maestro 10.3⁷⁶, followed by MD simulations and MM-GBSA analysis. First, a combinatorial library including 256 ligands for DHE and 64 ligands for ERG was prepared using the Interactive Enumeration program. The variants were defined by establishing substitution sites where there were four possible points of substitution to DHE and three possible points of substitution to ERG. At each possible point of substitution there were 4 functional groups that can be substituted which included hydrogen, fluorine, chlorine, bromine. This suggests that there are 4⁴ possible modified versions of DHE and 4³ possible modified versions of ERG, and a combinatorial library of these 256 ligands for DHE and 64 ligands for ERG was generated. The charge of each compound at pH=7 was determined by Epik (an empirical pKa prediction program)⁴⁷ followed by a geometry optimization that minimized the potential energy using the default parameters. Using the active receptor structure from the most abundant conformation of each system, a grid file was generated using the Receptor Grid Generation program to prepare the complex for the subsequent docking calculation. In each system, ergotamine or dihydroergotamine was selected and a grid box was generated around the ligand with a Van der Waals radius scaling factor of 1.0 and a partial cutoff of 0.25. Then, these 256 ligands for DHE and 64 ligands for ERG compounds were docked using Glide with Extra Precision (XP) scoring function, and then filtered using OikProp package⁷⁷, to predict the absorption, distribution, metabolism, and excretion (ADME) properties. QikProp ranks the full molecular structure based on pharmaceutically relevant properties by giving each compound a number of stars; compounds with no starts are predicted to be the most drug-like. Finally, three potential compounds for each ligands were manually chosen based on XP scores (< -9.0 kcal/mol)

that were more negative than the docking of ERG or DHE into the active conformation of 5HT_{1B} from the most abundant clusters, along with the compounds' synthesizability containing fewer substitution groups. The five XP docking complexes were subjected to 200 ns MD simulations. MM-GBSA binding energies from the last 100 ns simulation were then calculated and compared.

Results

Table 1 MM-GBSA binding energies of ergotamine and dihydroergotamine to the 5-HT_{1B} receptor.

	ΔVDW^1	ΔLIPO^2	ΔGBELE ³	$\Delta \mathrm{E}^4$	ΔOriginal ⁵
ERG Original	-68.6±4.9	-61.6±4.7	-36.2±4.6	-166.5±11.2	0
ERG Compound 1	-70.9±3.8	-46.7±3.8	-65.9±3.0	-183.4±6.7	-16.9
ERG Compound 2	-70.9±4.3	-44.7±4.1	-67.5±2.9	-183.1±6.5	-16.6
DHE Original	-66.2±3.3	-53.7±2.6	-31.7±3.0	-151.6±6.2	0
DHE Compound 1	-71.1±2.1	-41.9±6.1	-59.3±2.2	-172.3 ± 6.6	-20.7
DHE Compound 2	-65.1±3.5	-52.7 ± 5.4	-51.3±2.9	-169.1±8.2	-17.5
DHE Compound 3	-70.9±4.6	-43.0±5.3	-60.2±3.8	-174.2±9.4	-22.6

¹ ΔVDW: Change of van der Waals energy (VDW + π - π stacking +Self-contact correction) in gas phase upon complex formation 2 Δ LIPO: Change of lipophilic term (Lipophilic energy) upon complex formation.

Our MM-GBSA binding energy data indicates that ERG binds stronger than DHE to the 5-

HT_{1B} receptor. MM-GBSA calculations were performed in order to compare the ligand binding affinities of both drugs with the receptor. Table 1 shows, ERG shows an overall stronger MM-GBSA binding energy by -15 kcal/mol. Individually, van der Waal (-2.4 kcal/mol), lipophilic (-4.5 kcal/mol), and electrostatic interaction (-7.9 kcal/mol) energies were all weaker for DHE then ERG. This is qualitatively consistent with activity data for the drugs where ERG has higher binding affinity (p $K_i = 8.69$) compared to DHE (p $K_D = 7.85$).

³ ΔGBELE: Change of electrostatic interactions (GB/Generalized Born electrostatic solvation energy+ ELE/Coulomb energy +Hydrogen-bonding) upon complex formation.

⁴ ΔE: MM-GBSA binding energy (Complex – Receptor – Ligand).

⁵ ΔOriginal: Change between either ERG or DHE and their respective new compounds

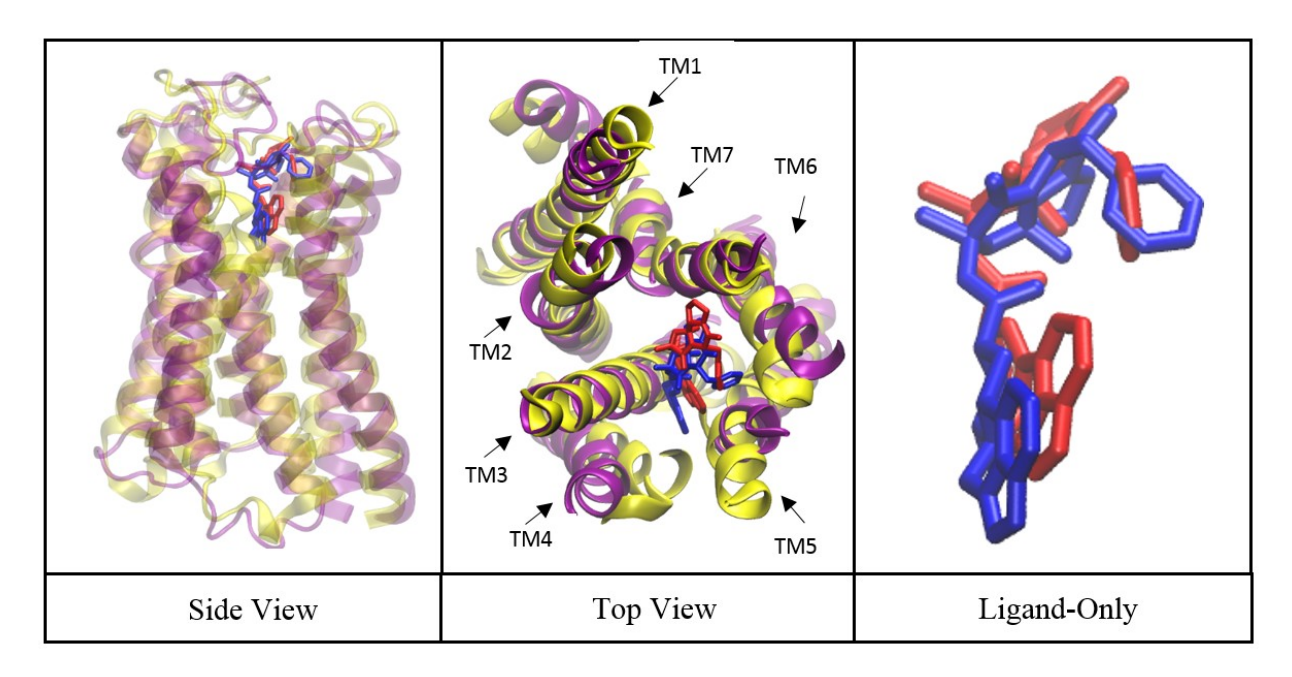


Figure 2 Comparison on the representative structure of the most abundant cluster from the MD trajectories of the two complexes (5-HT_{1B}/yellow//ergotamine/red and 5-HT_{1B}/purple//dihydroergotamine/blue).

The two active complexes (ERG-5-HT_{1B} and DHE-5-HT_{1B}) are structurally similar. After identifying the major binding poses as described in the methods, additional analysis was done on both ligand complexes. For comparison, we superimposed the representative structure of the most abundant cluster of each complex. Figure 3 shows a side view, a top view, and only the ligands for appraisal. Figure S4 similarly shows superimposition of the most abundant MD complexes with the crystal complexes. As these views show, the complexes have subtle differences in most cases but lacks major configurational changes.

Table 2. Key residues of 5-HT^{1B} interacting with ERG and DHE, with MM-GBSA decomposition analysis (better than -2.0 kcal/mol), and difference in binding energies of DHE and ERG.

Residue # Ergotamine (Contact #, kcal/mol)		Dihydroergotamine (Contact #, kcal/mol)		Difference in bonding energy (kcal/mol) ¹	
N Terminal	Y38 (0.139)	,	Y38 (0.120)	,	
N Terminal					Y40 (1.55)
3.26		D123 (-2.5)			
3.28	W125 (0.153)		W125 (0.117)		
3.29		L126 (-2.2)	L126 (0.058)	L126 (-2.6)	
3.32	D129 (2.068)	D129 (-17.3)	D129 (2.121)	D129 (-17.8)	
3.33	I130 (0.165)	I130 (-7.1)	I130 (0.250)	I130 (-7.9)	
3.36	C133 (0.148)		C133 (0.394)		
3.37	T134 (0.180)		T134 (0.603)		
4.57	S181 (0.152)				
ECL2					K191 (1.59)
ECL2	E198 (0.063)	E198 (-1.0)			
ECL2		C199 (-2.0)			
ECL2	V200 (0.089)	V200 (-5.1)	V200 (0.051)	V200 (-3.5)	V200 (1.55)
ECL2	V201 (0.968)	V201 (-7.5)	V201 (.901)	V201 (-5.6)	V201 (1.88)
ECL2				D204 (-2.1)	D204 (-1.12)
5.39			Y208 (0.081)		
5.40					T209 (-1.95)
5.41			V210 (0.480)		
5.43	S212 (0.147)	S212 (-4.3)			S212 (2.76)
5.44		T213 (-2.4)		T213 (-5.9)	T213 (-3.51)
5.46	A216 (0.080)		A216 (0.360)		A216 (-1.03)
5.47			P217 (0.272)		
6.48	W327 (0.221)	W327 (-1.0)	W327 (0.308)		
6.51	F330 (0.832)	F330 (-7.0)	F330 (0.361)	F330 (-2.5)	F330 (4.43)
6.52	F331 (0.880)	F331 (-2.0)	F331 (0.198)		F331 (1.84)
6.54	I333 (0.046)				
6.55		S334 (-2.3)			S334 (1.17)
6.58	M337 (0.230)	M337 (-4.1)			M337 (4.06)
6.59			P338 (0.136)		
6.60			I339 (0.205)		
ECL3			C340 (0.170)	C340 (-2.4)	C340 (-2.33)
ECL3	K341 (0.035)		K341 (0.091)		
7.31	L348 (0.143)	L348 (-3.3)			L348 (2.85)
7.34	F351 (0.270)	F351 (-4.7)	F351 (0.134)	F351 (-2.8)	F351 (1.84)
7.35	D352 (0.087)	D352 (-5.9)		D352(-5.3)	
7.38	T355 (0.636)	T355 (-2.8)	T355 (0.613)	T355 (-2.0)	
7.42	Y359 (0.076)		Y359 (0.079)		

Top contributors to the bonding energy difference between DHE and ERG.

The protein-ligand interaction analysis shows that the key protein-ligand residual contacts in ERG are conserved in DHE, but they exhibit different bonding energies. A SID analysis was preformed, aforementioned in the methods, to identify key residues in the 5-HT_{1B} receptor involved with ERG and DHE bindings. All residues in the table are assigned the Ballesteros-Weinstein number for the receptor ⁷⁸. The significant 5-HT_{1B}-ERG interactions include a total of 23 residues from N-terminal, TMs 3, 4, 5, 6, and 7, and extracellular loops 2 and 3 (Table 2). For 5-HT_{1B}-DHE, there are also 23 key residues from N-terminal, TMs 3, 5, 6, 7, and extracellular loops 2 and 3. Even though the majority of the key residue interactions are conserved for each ligand, there are limited observed differences of the interaction fractions for each of the complexes. Interaction fractions for each residue in both complexes remain similar, with exception to P331^{6.52} and P330^{6.51}, which were highly conserved in ERG but not in DHE. The MM/GBSA energy decomposition was used to identify key residues that contribute more than -2.0 kcal/mol (Table 2). There is some evidence of overlap with the contact analysis. Several additional key residues were identified: A123^{3.26}, L126^{3.29}, C199^{E2}, T213^{5.44}, and S334^{6.55} for ERG; A204^{E2}, T213^{5.44}, and A352^{7,35} for DHE. Also, the difference in MM/GBSA energy decomposition was calculated between DHE and ERG, with ERG binding stronger at residues V200^{E2}, V201^{E2}, S212^{5.42}, F330^{6.51}, F331^{6.52}, M337^{6.58}, L348^{7.31}, and F351^{7.34}, which correlates with mostly hydrophobic interactions. On the other hand, DHE bound stronger at residues D204 E2, T209^{5.39}, T213^{5.43}, A216^{5.46}, and C340^{E3}. The significant differences in MM/GBSA bonding energies correlate with the identified key residues, which suggests that these residues have a strong contribution to the absolute bonding energy with each ligand. A number of these residues are involved in known binding features of the 5-HT_{1B} receptor. For example, N-terminal residues such as Y40^{N-Term} are known to fold over the top of the binding pocket to enhance binding interaction and is thought to play a role in ligand recognition¹⁶. Residue D129^{3,32} is known to anchor the ergoline scaffold through a salt bridge and this interaction is further stabilized through hydrogen binding with Y359^{7,43}. A hydrogen bond is

formed between the indole N-H Hydrogen of ergotamine and T134^{3.37}. In addition, a hydrophobic cleft is known to form from the side chains of C133^{3.36}, I130^{3.33}, W327^{6.48}, F330^{6.51}, and F331^{6.52}
¹⁶, all of which are observed in our two-dimensional interaction diagrams.

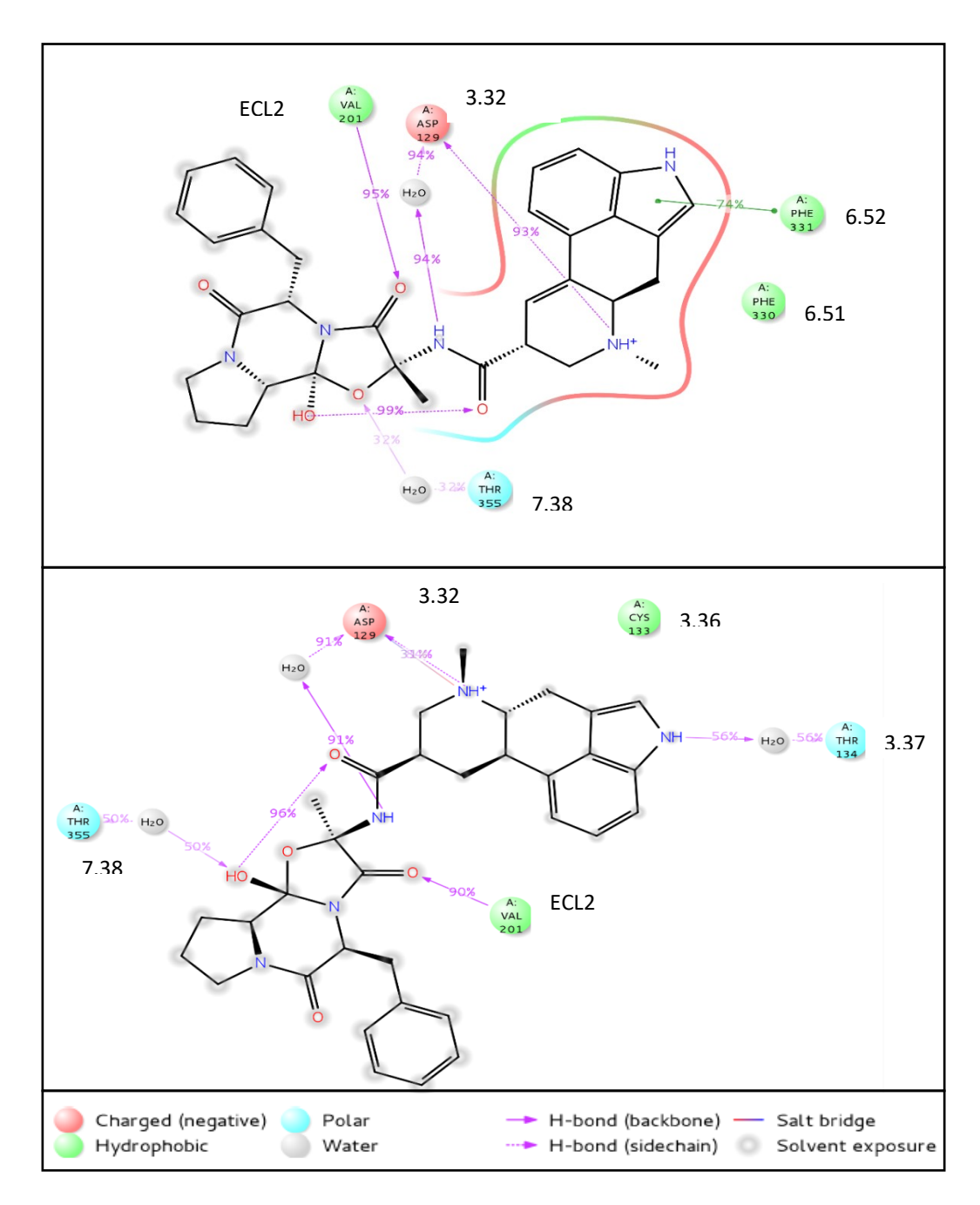


Figure 3 Ligand-residue interactions that persist for more than 30% of MD simulation time for ergotamine (top) and dihydroergotamine (bottom) with 5-HT_{1B}. Ballesteros-Weinstein numbering is annotated for each interacting residue.

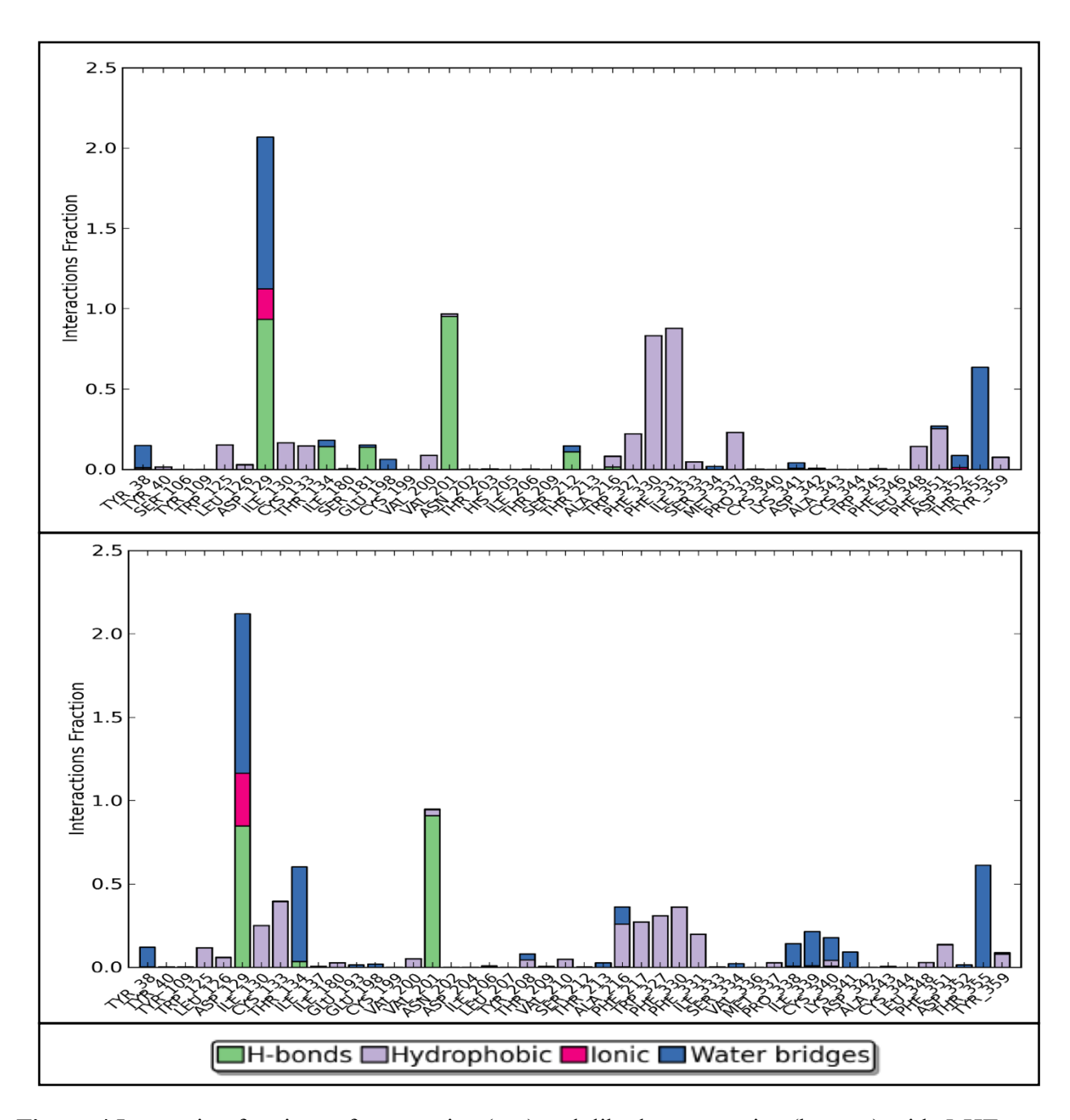


Figure 4 Interaction fractions of ergotamine (top) and dihydroergotamine (bottom) with 5-HT_{1B} over the MD trajectory.

The ligand-residue analysis shows subtle differences between ERG and DHE. To identify the critical interactions the drugs made with the protein, SID analysis was conducted as described in the methods. The major interacting residues are outlined in Table 2 and visually represented in Figures 3-4 and Figure S5. Table 2 also contains Ballesteros-Weinstein numbering and interaction fraction⁷⁸. Some noteworthy differences between the two drugs include: A) A much higher

interaction fraction with THR134^{3,37} and DHE compared to that residue with ERG. B) A greater interaction fraction at residues PHE330 and PHE331 in ERG. C) A significant interaction fraction for water bridges between residues 338-341 of DHE not seen in ERG. It should also be noted that ASP129^{3,32} has the greatest interaction fraction for both ligands. That fraction remains fairly consistent for both ligands, with ERG's being 2.068 and DHE's at 2.121.

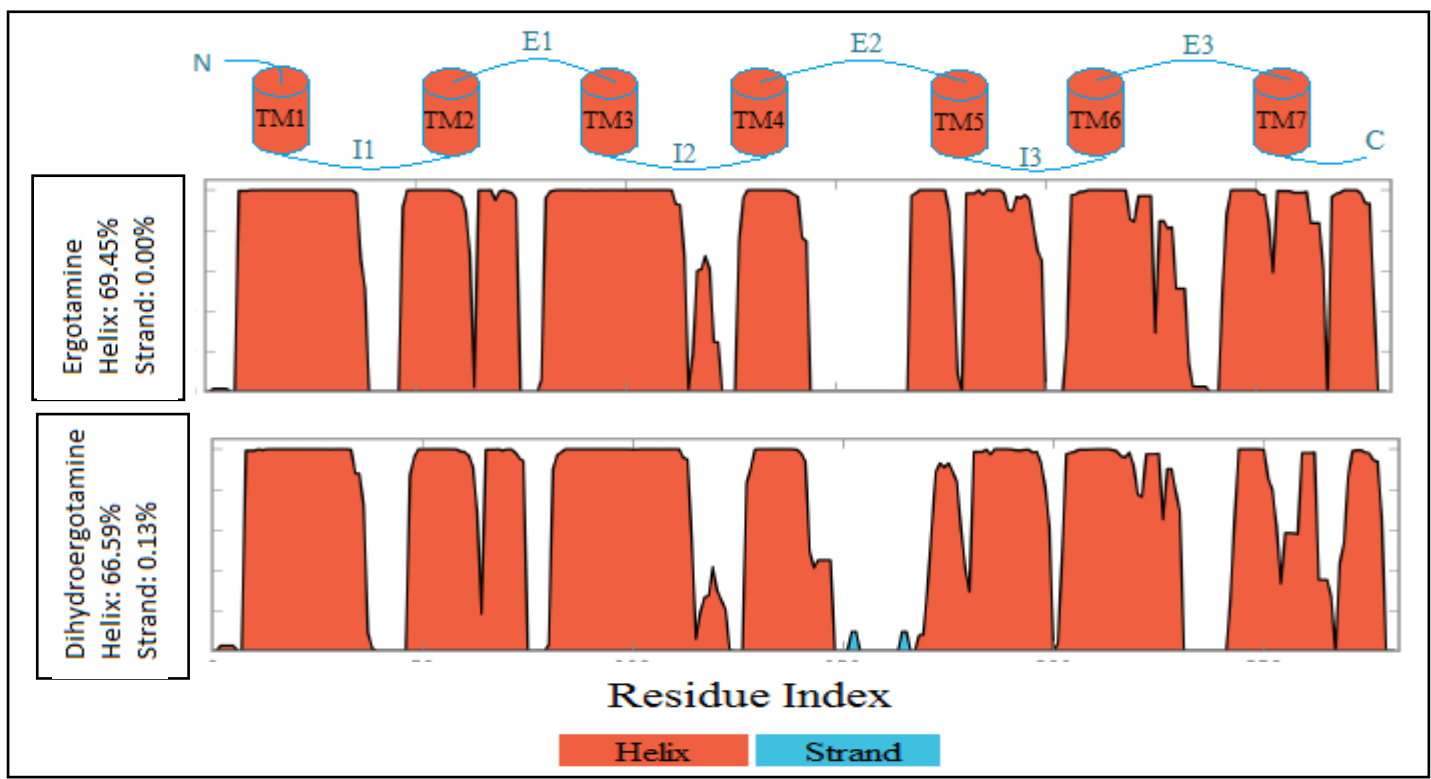


Figure 5 Comparison of the secondary structure percentage of each protein residue between Ergotamine system and Dihydroergotamine system. Overall SSE percent contribution is annotated.

An examination of secondary structures shows that helices are maintained but still contain subtle differences. The shape, abundance over the MD trajectory, and time evolution for the two secondary structures are shown in Figure 5. Some notable features include: A) Presence of very short β -strands in DHE between transmembrane four and five. B) Additional kinks in DHE from transmembrane 7 to the C-terminal.

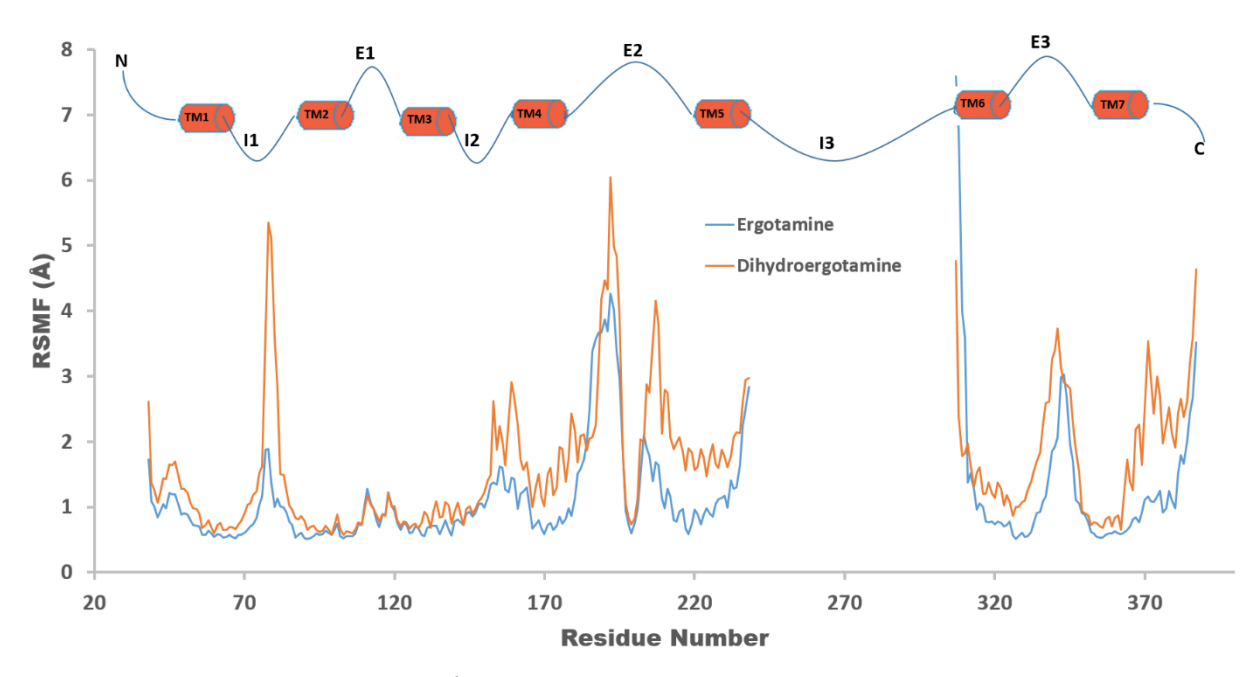


Figure 6 Receptor protein RMSF (Å) diagram of 5-HT_{1B} with the two ligands, ergotamine and dihydroergotamine, from MD simulations.

The receptor RMSF data shows that the receptor have differences in flexibility when interacting with different ligands. The receptor RMSFs for the different ligands is shown in Figure 6. Because the intracellular loop three that was missed in the crystal structure was not included in the simulations, its RMSF was not available for both systems. In general, this figure shows that the more rigid components of the receptor, such as the helices, have lower RMSF. In contrast, more flexible areas like the intra and extra cellular loops and the N- and C- terminals have high RMSF values. While the shape of the curves across residue numbers is generally consistent between the ligands, there is a marked contrast in size. DHE has higher RSMF throughout almost every transmembrane and intra and extra cellular region. Some major areas of contrast are seen at intracellular region one, intracellular region two, extracellular region two, and the C-terminus. These differences emphasize the receptor increased flexibility when interacting with more flexible DHE than ERG, this is likely the main factor at receptor level contributing to the biological and activity differences caused by the two drugs.

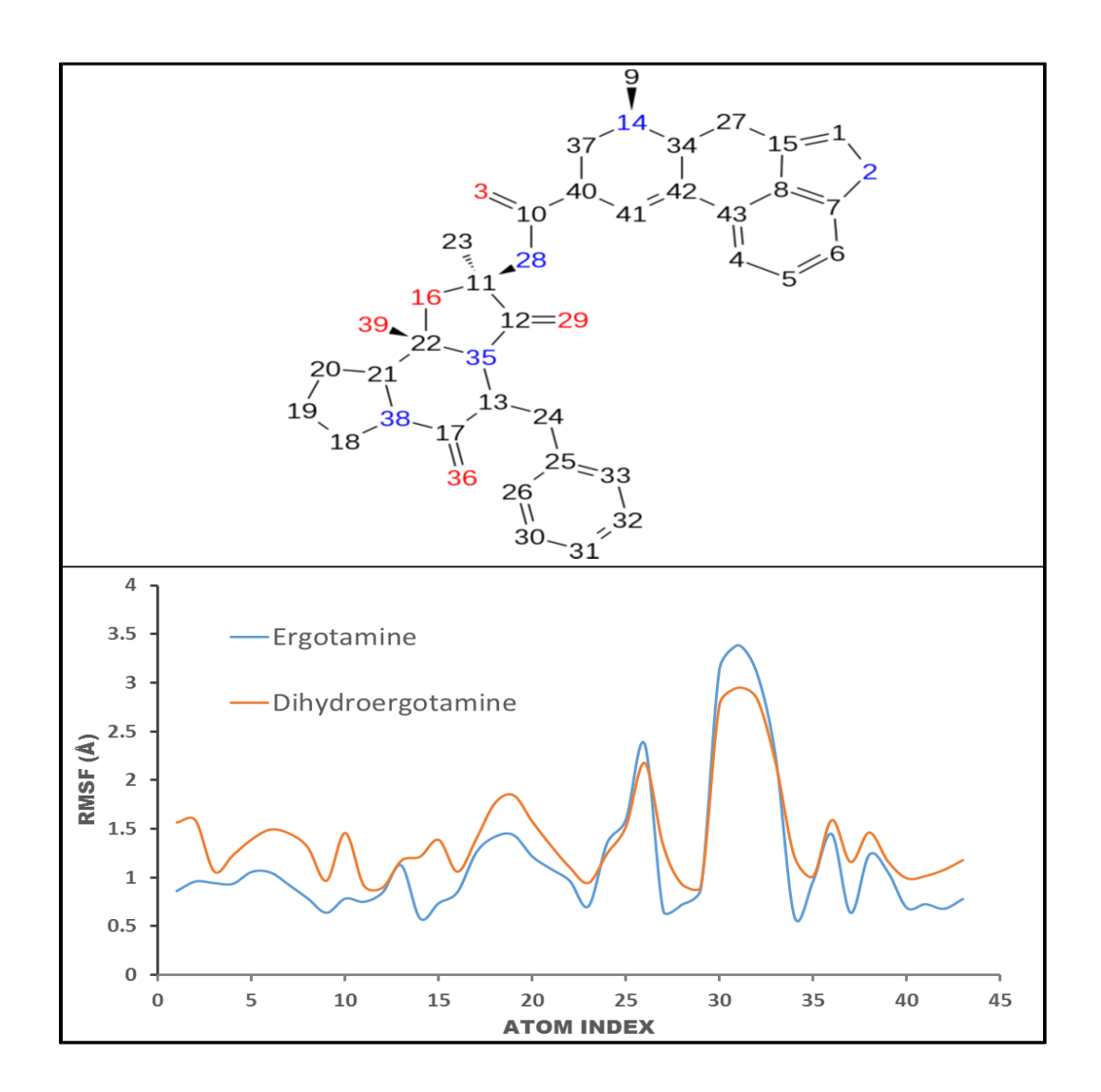


Figure 7 Ligand RMSF (Å) diagram of 5-HT_{1B} with the two ligands, ergotamine and dihydroergotamine, from MD simulations. The two ligands have the same atom numbering, but only ergotamine is shown here.

A trend of higher ligand position fluctuation was also observed for DHE. Ligand RMSF can be used to gain a sense of how the ligand conformation dynamics between the drugs differ. Figure 7 shows that ERG has lower RMSF values at almost all atoms. It is only around atom 25 and atom 32 in the phenol ring that its RMSF value is greater than that of DHE. This is consistent with what was expected from the structures of the two drugs – ERG, which contains one more π bond then DHE, is overall the more rigid ligand compared to DHE's flexibility.

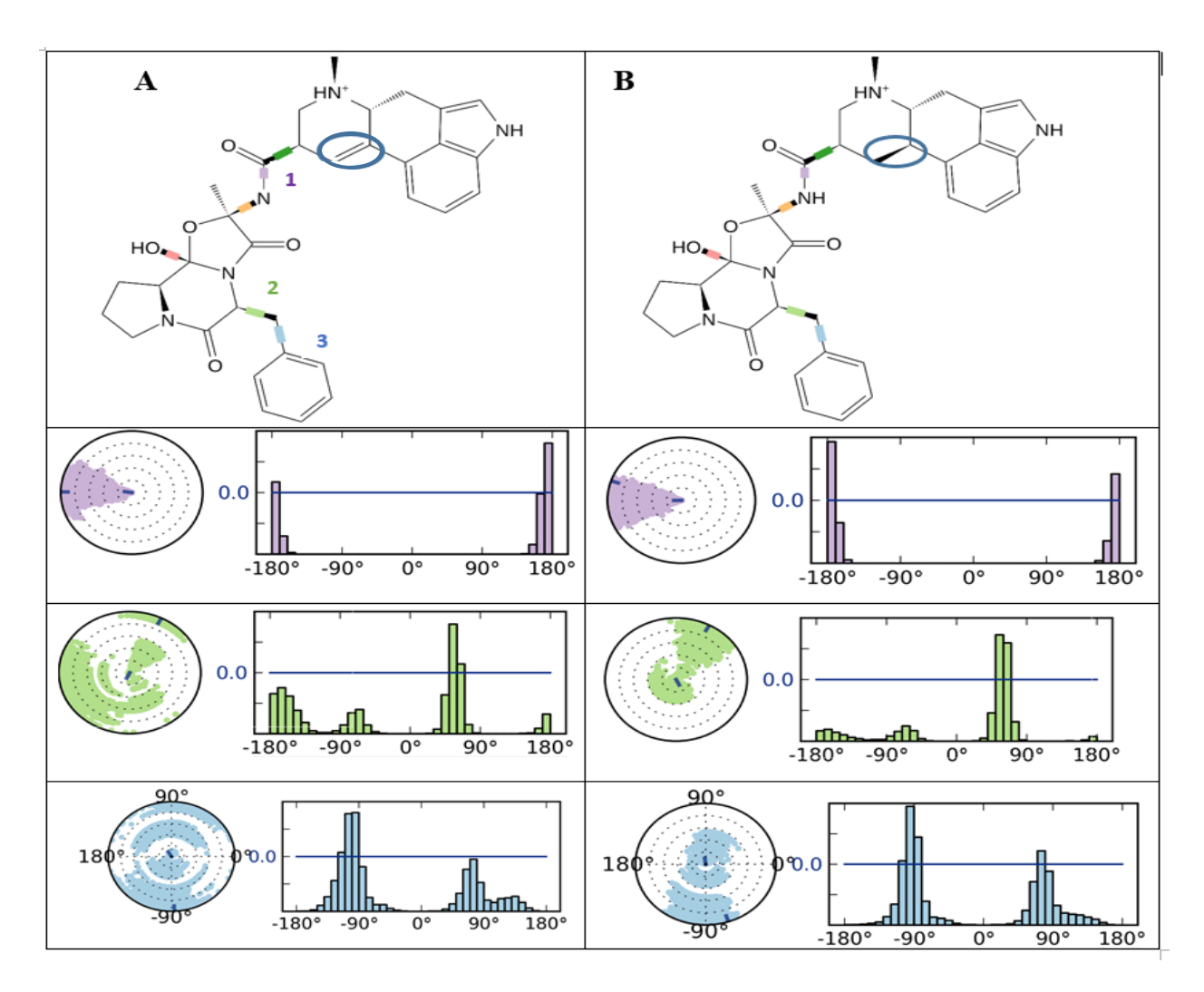


Figure 8 Ligand torsion plots showing the average conformational evolution of three rotatable bonds throughout the MD trajectory for ergotamine (A) and dihydroergotamine (B). The color of the plots correspond to the color of the rotatable bond.

Ligand torsion plots further illustrate difference in rotational mobility at the two linkers between the ligands. The hydrogenation of a double bond in DHE changes the rotational flexibility of the rotatable bonds at the two linkers of the ligand. While many of the bonds retained similar conformational evolution throughout the MD trajectory for both ligands, three bonds at the two flexible linkers did exhibit some clear changes as shown in Figure 8. This indicates the small ligand modification can lead to subtle allosteric effects away from the change origin. Additional torsional angle plots can be found in Figures S5-S6.

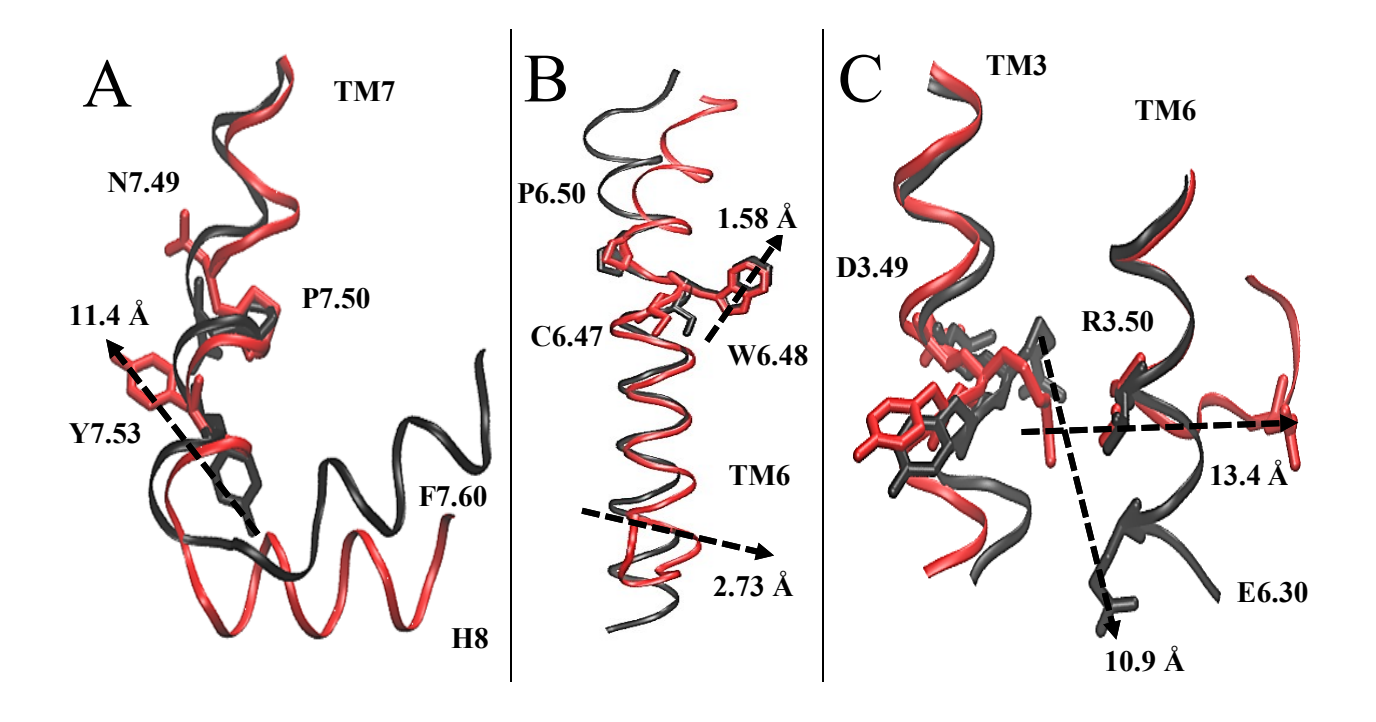


Figure 9 A. Tyr Toggle Switch (NPXXY) (ERG: red/DHE: black) shown with a moving distance of 11.4 Å for the tyrosine^{7.53} sidechain. **B.** Transmission Switch (CWXP) (ERG: red/DHE: black) shown with a moving distance of 1.58Å for the tryptophan^{6.48} sidechain, and a moving distance of 2.73 Å for the TM6 helix. **C.** Ionic Lock Switch (DRY), (ERG: red/DHE: black) shown with difference of salt bridge bond lengths of 10.9Å (DHE), and 13.4 Å (ERG). All residues are labeled using the Ballesteros-Weinstein numbering system.

Micro-molecular switch analysis suggests while the tyrosine toggle switch, the transmission switch and the ionic lock are activated in 5-HT_{1B}-ERG, only the latter two switches are on in 5-HT_{1B}-DHE. Class A GPCRs share a set of conversed residues that are considered to be important in the receptor activation. For HT_{1B}, three such motives are considered to be critical in regulating its activity⁷⁹: NPXXY (in which X represents any amino acid) in TM7, CWXP in TM6 and DRY in TM3. We compared the structural aspects of these three molecular switches in the two HT_{1B}-ligand complexes (Figure 9). For the Tyr toggle switch (NPXXY), 5-HT_{1B}-DHE is in an active state, while 5-HT_{1B}-ERG is shown in the inactive state⁷⁹. The transmission switch (CWXP) does not show a significant difference between the two complexes with an agonist, it is likely that both

are in the inactive state. At the ionic lock switch (DRY), both 5-HT_{1B}-ERG and 5-HT_{1B}-DHE are shown as in an active state, due to the breaking of the salt bridge bond (13.4 Å and 10.9 Å). The micro switch analysis also includes a comparison of both ERG and DHE with the 5-HT_{1B} antagonist methiothepin (PDB: 5V54) (Figure S8 and S9)⁸⁰. ERG is inactive, while DHE is active for the Tyr toggle switch (NPXXY). For the ionic lock switch (DRY), both ERG and DHE show an active conformation when compared to the antagonist. At the transmission switch (CWXP), there is no significant conformational changes between the two systems and the antagonist, which could indicate an inactive state.

The dynamic network model identified subtle differences between the DHE and ERG systems at TM5 and TM6. Unweighted networks and network models weighed on the basis of the correlated motion in the simulation trajectory for the DHE and ERG systems (Figure S10 and Figure 11) were calculated as described in the method section. When comparing the unweighted network models of DHE and ERG systems, it is clear that there is a good agreement in terms of connection. However, when the correlation between the nodes are quantified in the weighted network model (Figure 10), differences are observed between the two systems. Most notably are the edges that surrounds TM5 and TM6, and are next to the binding pocket. The DHE system shows very high correlations between edges in TM5 and TM6 compared to the ERG system which shows extremely low correlated connections as depicted by the much thicker edges. Subtle differences were also observed at TM4 where ERG shows much smaller correlation between nodes around intercellular loop 2.

The weighted network model was then used to generate a community network model (Figure 10) which grouped together residues that interact more frequently and stronger than to residues in other communities. Figure 10 showed clear differences between the DHE and ERG systems. Specifically, ERG showed one large network (dark blue) with rigid connections

surrounding the entire binding pocket, whereas the DHE system has the binding pocket broken into three different communities. Critical edges were also generated which linked communities together (Figures 10 and 12) and those critical residues were identified (Table S1).

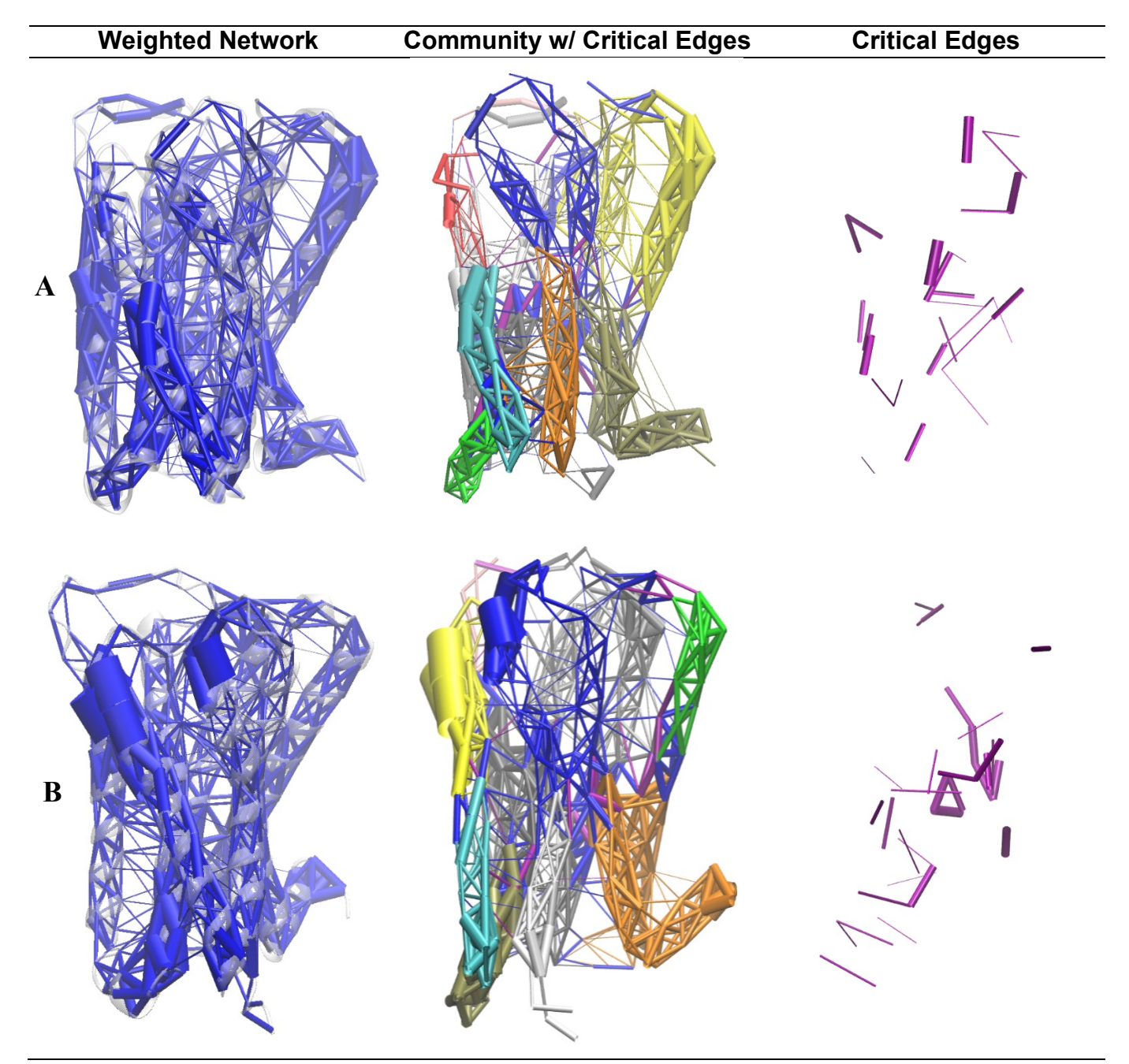


Figure 10. The dynamic network models weighted by correlation motion, each of the receptors structural communities separated by a different color and the critical edges shown in purple for the DHE (A) and ERG (B) complex systems.

Optimal paths revealed key residues involved in the shortest pathway for passing a signal from DHE or ERG to the site of the molecular switch. From the weighted network models, the shortest pathway able to pass a signal from the ligand (DHE or ERG) to the site of each molecular switch (Tyrosine Toggle Switch: Ile384, Transmission Switch Ala312, Ionic Ala150) was calculated as the optimal path (Figure 11). Although there are similarities between the two systems, most notably for the Ionic Lock (DRY) each optimal path generated is unique. For the Tyrosine Toggle Switch (NPXXY), DHE's optimal path sends signals primarily along TM1, TM2 and TM3, whereas ERG's optimal path goes primarily through TM7. Also consistent with our micro-switch analysis, the Transmission Switches (CWXP) for both DHE and ERG are very different where ERG shows to have a much more direct path of communication.

In order to check the convergence of our simulation systems, we extracted the last 800 ns of each system as indicated from the RMSD (**Figure S2**). This 800 ns portion of the trajectories were split into two blocks of 400 ns each and subjected to individual network analyses (**Figure S14**). Evident from these figures, the combined trajectories were nearly identical to the trajectory blocks. Optimal paths were also generated for the trajectory blocks which showed identical optimal paths as in the combined trajectory.

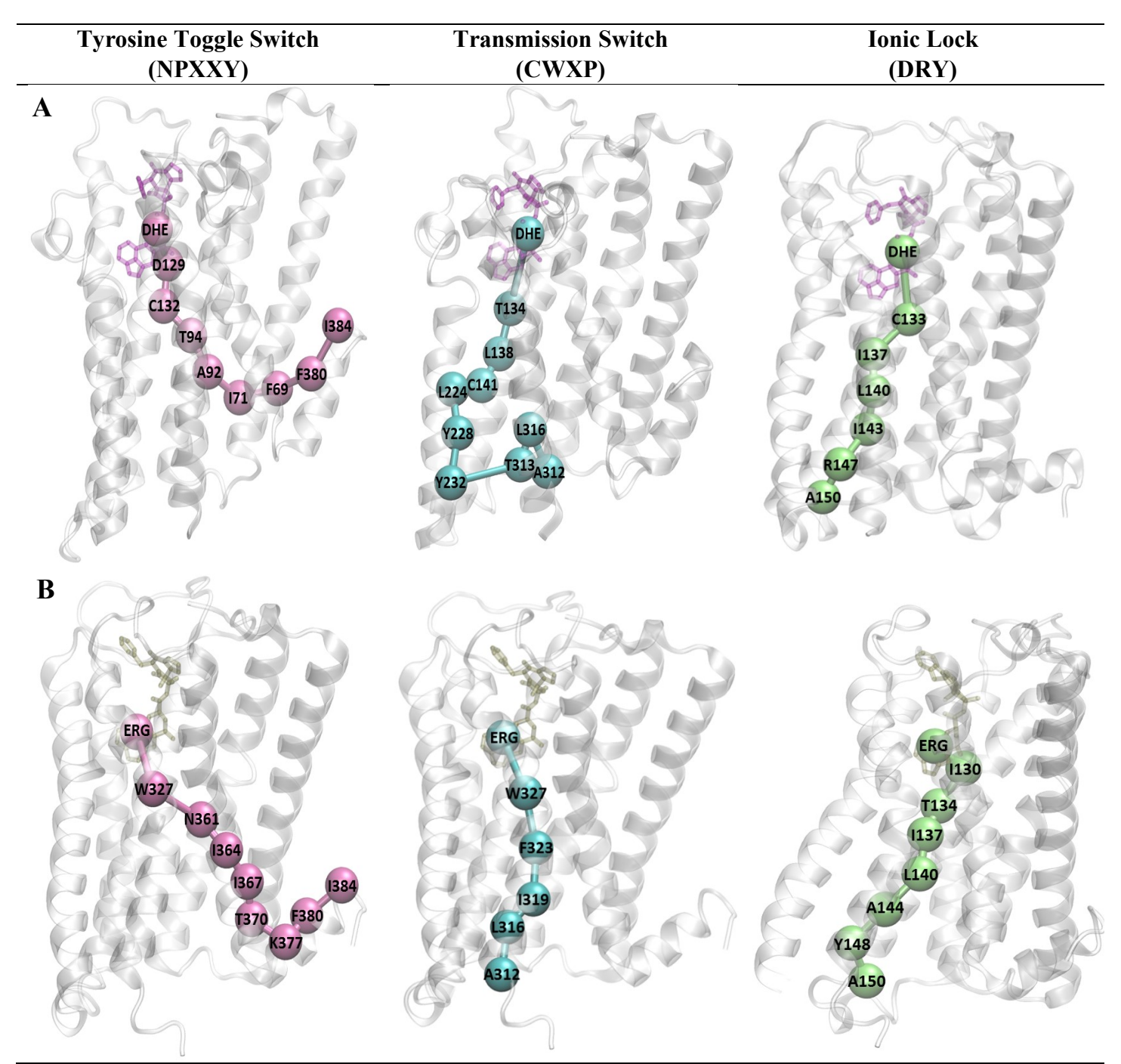


Figure 11. The shortest path generated for each major molecular switch observed in the MD simulations of the DHE (A) and ERG (B) complex systems.

Referencing the critical nodes with mutagenesis data identified residues that may play an important role in the receptor activation of for each system. From the community analysis (Figure 10) there were 45 critical nodes identified for the DHE system (Figure 12 A-B), 40 for the ERG system (Figure 12 C-D) and 13 identified to be critical nodes in both systems (Figure 12 E-F). Since the critical nodes were involved in signal transduction between different parts of the receptor in our simulations, the critical residue information was then referenced with experimentally reported mutagenesis data available on the G-protein coupled receptor databank (GPCRdb) to see if there residues were involved in the physical signal transduction (Figure 13; Figure S11). There were 15 critical residues that overlapped with natural or in vitro mutations of the 5-HT_{1B} receptor. The DHE system had nine critical residues were also mutations (I71^{1.54}, A92^{2.47}, V93^{2.48}, T134^{3.37}, C141^{3.44}, F185^{4.61}, V200^{45.51}, W327^{6.48}, F331^{6.52})^{16, 81, 82}, ERG had 10 $(S45^{1.28}, T60^{1.43}, A92^{2.47}, C141^{3.44}, W327^{6.48}, F331^{6.52}, Y359^{6.52}, S362^{7.43}, P366^{7.50}, Y369^{7.53})^{16,\,81,\,81}, Y369^{7.53})^{16,\,81}, Y369^{7.53}, Y369^{7.53})^{16,\,81}, Y369^{7.53}, Y369$ 82 , and four were conserved between the two systems (A92^{2.47}, C141^{3.44}, W327^{6.48}, F331^{6.52}). We speculate that the four conserved residues may be critical for the activation of the receptor, whereas the differences may help to explain the different potencies of the two drugs.

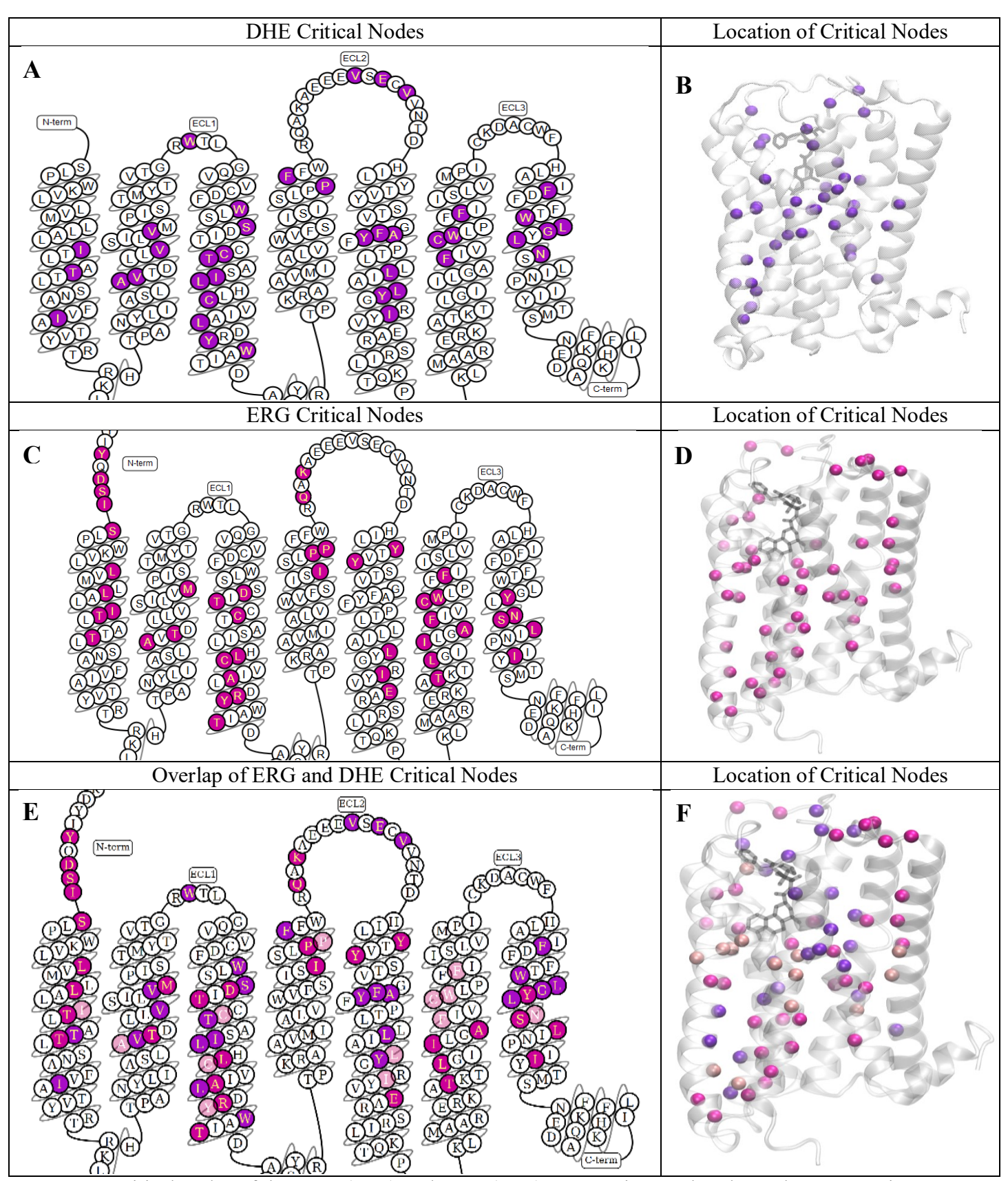


Figure 12. Critical nodes of the DHE (A-B) and ERG (C-D) systems in a snake plot and structure view. A plot comparison between the two system in presented in E-F where purple represents DHE, dark pink represents ERG, and the light pink residues are those that are conserved in both systems.

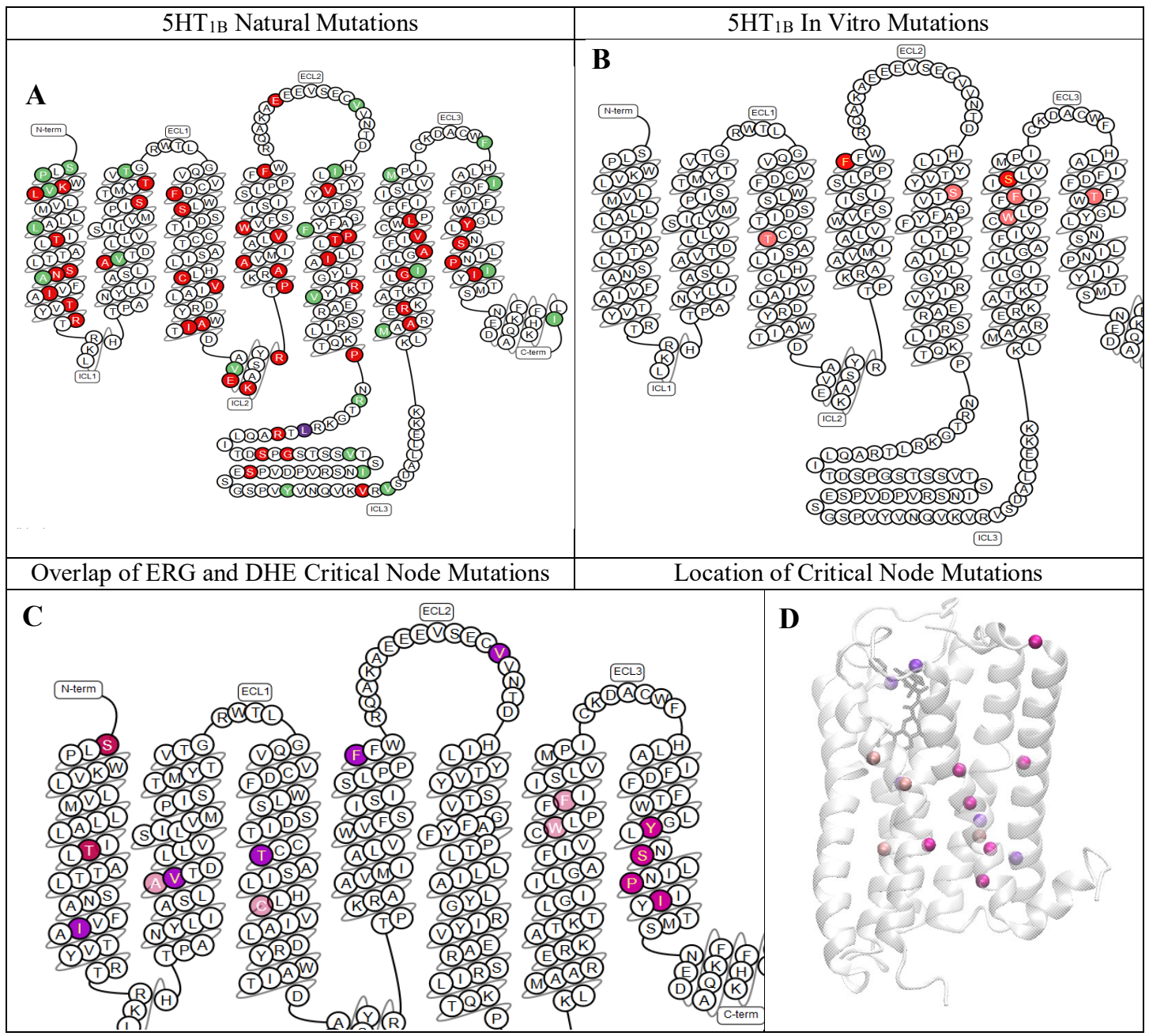


Figure 13. Reported mutagenesis data for the 5HT1B receptor. Mutated residues in red cause decrease in activity, green cause increase in activity and purple is a deleterious stop gained mutation (A-B). The critical nodes that overlapped with the mutation data are in C-D where purple represents DHE, dark pink is ERG, and light pink represents the overlap between DHE and ERG.

Discussion

The structures of DHE and ERG share many similarities - a characteristic that can be clearly seen when the ligands are superimposed (Figures 3, S3). Yet, other studies have found clear

activity differences between the ligands at many receptors. This study aimed to use molecular dynamics to better understand why such activity difference occurs at 5-HT_{1B}. Molecular dynamics is widely known to complement experimental data by illuminating functionally relevant characteristics of the ligand-protein interaction ¹⁷. Specifically, simulations can provide information about dynamic motion that may be otherwise hard to model. Proteins exist in a natural state of fluctuation, making an understanding of dynamic motion essential to understanding specific functions of a biomacromolecule ⁸³. Thus, our dynamic analyses such as the protein and ligand RMSF, micro switch analysis, dynamic network models, and normal model analyses sought to determine whether an understanding of these fluctuations could illustrate the activity differences between DHE and ERG. Following this, based on the dynamic information gained from our analyses, we also suggest possible modifications to both DHE and ERG that may enhance their binding at 5-HT_{1B}.

Molecular dynamics (MD) simulations were performed on each complex and the resulting trajectories analyzed and compared. ERG showed stronger MM-GBSA binding energy and much less flexibility than DHE. There were also significant differences in bonding energies at several key residues, the majority of which indicated that ERG showed a higher bonding energy to the receptor than DHE. The receptor protein and ligand RMSF both illustrate the tighter binding of ERG to 5-HT_{1B}. The ligand torsion plots illustrate how the introduction of an extra π bond can cause clear changes in the rotatable bonds of the system. Furthermore, interaction diagrams indicate that the ligands have some similar, but many distinct, interactions with its environment. Evaluations of several molecular switches were preformed using the most abundant conformation from the MD simulations. A study by reported on the distance of the ionic lock switch on a mutant β 2AR GPCR with a distance of approximately 13 Å, indicating complete breakage. The 5-HT_{1B} - ERG has a salt bridge bond distance of 13.4 for the ionic lock switch (DRY), much like the distance

in an activated B2AR receptor. The conformation state in the ionic lock switch (DRY) showed evidence that both 5-HT_{1B}-ERG and 5-HT_{1B}-DHE had broken the salt bridge bond and was in the active state. It appears both 5-HT_{1B}-ERG and 5-HT_{1B}-DHE are in the inactive state conformation for the transmission switch when compared to an antagonist. The Tyr toggle switch (NPXXY) shows a significant difference in the molecular switch state of 5-HT_{1B}-DHE and 5-HT_{1B}-ERG. 5-HT_{1B}-ERG is shown in an inactive state, while 5-HT_{1B}-DHE is shown in an active state. The difference in the Tyr toggle switch provides a possible mechanism for why ERG is more potent than DHE.

Dynamic network models based on MD simulations data are an efficient manner to extract correlated motions, allosteric signals and signal transduction networks within a complex system. This is useful because these correlation motions are likely linked to their activity and are normally hard to accurately discern through visualization of the MD simulations alone^{41, 42}. Furthermore, the dynamic networks allow different regions of the complex system to be clustered into highly correlated communities which can provide insight into the effect of ligand binding to the overall communication network ^{41, 43, 44}. In our study, significant differences were identified between the DHE and ERG complex systems in the dynamic network analysis. Specifically, when comparing the original unweighted dynamic network (Figure 10) to the connections between nodes in the networks that were weighted based on correlated motion in the simulation trajectories. The nodes of the ERG system have a significantly lower covariance, as shown by the thicker edges between nodes. In addition, the community models show that the ERG system is composed of less communities, and significantly different critical nodes, which pass information between the various communities. Specifically, ERG showed one large network (dark blue) with rigid connections surrounding the entire binding pocket, whereas the DHE system has the binding pocket broken into three different communities (Figure 10), indicating that the residues

surrounding the 5-HT_{1B} binding pocket are highly correlated when ERG is bound. Since the communities are grouped together based on residues that interact more frequently and strongly with one another, this analysis highlights how the small structural difference between ERG and DHE can cause significant changes to the dynamics of the 5-HT_{1B}.

The optimal path generated for the molecular switches of each system also varied between systems (Figure S12). The subtle difference in the optimal paths for the Tyrosine Toggle Switch (NPXXY) may play a role in the difference of active and inactive states at the Tyr toggle switch (NPXXY) and may further indicate a different molecular signal transduction pathway involving each ligand. Additionally, the Transmission Switches (CWXP) for each system were noticeably different. Thus, we propose the residues identified from the optimal paths are involved in the signal transduction pathway leading to activation through the molecular switches and that DHE and ERG are using separate communication pathways for activation, which is consistent with what was inferred from our original micro-switch analysis.

Specifically, we identified residues A92^{2,47}, C141^{3,44}, W327^{6,48}, F331^{6,52} to be critical in the binding and communication pathway for both the DHE and ERG systems. Based on the comparison of our critical nodes to the experimental mutagenesis studies, these four residues were identified, as critical residues involved in both the transfer of information between different communities as well as residues that when mutated significantly affect the activity of the receptor. Building on this, for the ERG system's optimal path analysis, W327^{6,48} was the first residue involved in the predicted optimal signal transduction pathway for both the Tyrosine Toggle Switch (NPXXY) and Transmission Switch (CWXP). One study compared the crystal structure of an inverse agonist at the 5-HT_{1b} orthostatic binding pocket to ERG at the same binding pocket⁸⁰. Their analysis described the outward movement of residues W327^{6,48} and F331^{6,52} upon binding of an inverse agonist. Considering the results from our network analysis in combination with their

results, the importance of $W327^{6.48}$ and $F331^{6.52}$ in the active conformation of the receptor can be deduced.

From the normal mode analysis (Figure S12), modes 1-3, show the most difference in motion, which are the lowest energy modes identified from the principal component analysis. In our analysis we observed the DHE system having a higher degree of fluctuation and an overall distinct motion when compared to ERG. Through the normal mode analysis we were able to provide another level of insight into the intrinsic dynamics of these complexes in the lowest vibrational state. From this analysis we concluded that the overall intrinsic dynamics of the complexes are distinct of another which provides further support to our hypothesis that the activity differences of these complexes are due to differences in their dynamic interactions. Overall, this information, in combination with our other dynamic analyses such as the RMSF, dihedral angle distribution, and network models, help to explain the activity differences that cannot be explained from the crystal structure alone.

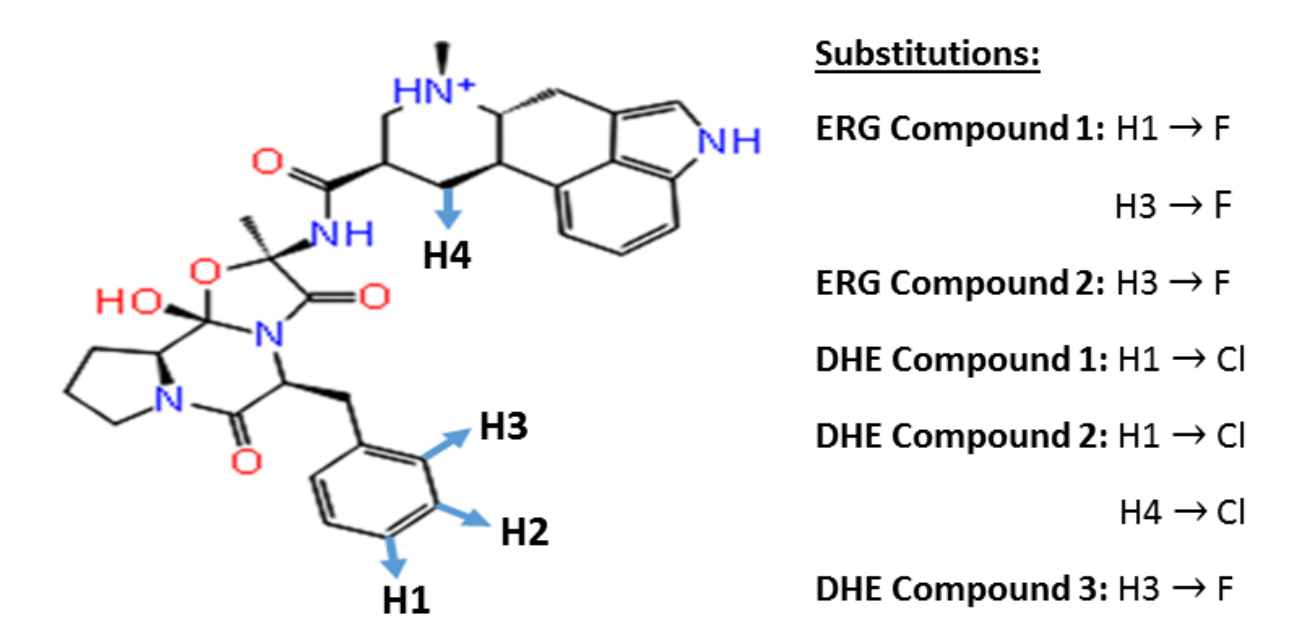


Figure 14. Substitutions made on the top compounds chosen from the high-throughput virtual screening. Dihydroergotamine's two dimensional structure is used as an example where the blue arrows represent possible substitution sites (A), and the actual substitutions are listed on the right (B).

Based on the dynamics insight gained from our MD simulations and post simulation analysis we suggest two major modifications possible for DHE and ERG. The first is at position 41 of dihydroergotamine (see **Figure 7** for reference to ligand positions). Evident from the comparison of ergotamine to dihydroergotamine in our protein (Figure 6) and ligand (Figure 7) RMSF, the overall RMSF is higher in the dihydroergotamine system. Thus we suggest that adding a small function group to carbon 41 could reduce the fluctuations and increase interactions at this site. Our second suggested set of modifications are based on our torsional angle distributions and our visual inspection of the most abundant poses. The torsional angle distribution shows for both ergotamine and dihydroergotamine the carbon 26-27 and 27-28 bond are highly flexible, and from a visual inspection of our simulations we observe this benzene bending outward toward the solvent upon binding. Thus, we speculate that adding small functional groups the 26th, 30th, and 31st positions of the benzene may enhance the potency of both ligands by reducing the fluctuations of this side chain through enhanced interactions in the binding pocket. At each possible point of substitution we picked 4 functional groups (hydrogen, fluorine, chlorine and bromine) that could be substituted leaving a total of 4⁴ possible modified versions of DHE and 4³ of ERG which we then used to generate a combinatorial library of these 256 ligands for DHE and 64 ligands for ERG. Each new compound was docked to the same orthosteric binding site as the most abundant cluster of DHE or ERG, with similar hydrogen bonds, π - π and hydrophobic interactions. The docking scores showed that of the 256 new compounds for DHE, 127 bound with a more favorable docking score than DHE (-6.85 kcal/mol), and of the 64 compounds for ERG, 59 docked more favorably than the original (-11.22 kcal/mol). Of these compounds, two compounds were chosen for ERG and three for DHE (Figure S15) based on their synthesizability determined by a minimal number of functional groups added, and more negative XP scores than ERG or DHE, respectively. Of these five compounds (Figure 14), Qikprop predicted that both ERG compounds 1 and 2 had zero stars,

DHE compound 1 had one star, and DHE compounds 2 and 3 also had zero stars, thus suggesting these molecules have suitable drug-like properties.

Since the docking scores were promising, the five complexes of these compounds were subjected to 200 ns MD simulations. The first post simulation analysis performed was the MM-GBSA calculations of the five systems (**Table 1**). Evident from this table each compound bound more favorably to 5-HT_{1B} than its original ligand. Specifically, for ERG, compounds 1 and 2 had binding energies that were -16.9 and -16.6 kcal/mol more favorable than ERG, respectively. Similarly, for the DHE compounds, compounds 1, 2, and 3 bound more favorably to 5-HT_{1B} by -20.7, -17.5 and -22.6 kcal/mol, respectively. Looking more into the MMGBSA, the VDW contributed the more to the total energy followed by the electrostatic and lipophilic interactions. Since in all but one compound, the VDW term increased when compared to the original ligand, we suggest there may be enhanced π - π stacking between residues of 5-HT_{1B} and the aromatic portions of the new compounds which were heightened after the addition of the functional groups.

Following the MM-GBSA calculation, our next post-simulation analysis was to compare the original ligands RMSF to the new compounds to see whether or not our prediction that adding functional groups would decrease the fluctuations of these ligands in complex with 5-HT_{1B} held true. As predicted, the protein RMSF (**Figure S16**) showed that the new compounds for both ergotamine and dihydroergotamine caused less fluctuations for the protein. Specifically, there was a significant decrease at TM5 for the ergotamine compounds and an overall decrease for the dihydroergotamine compounds. Further, the results of the ligand RMSF (**Figure S17**) clearly show a decrease in RMSF for both the ERG and DHE compounds. Importantly, this analysis clearly provided more evidence that our prediction of adding functional groups to the benzene ring would decrease the fluctuations of atoms on the benzene (i.e. 25, 26, 30, 31, 32, 33) could be true. Furthermore, this decreased fluctuation, which is likely due to an increase in

binding interactions and stability, is consistent with the improved MMGBSA binding energy of the top compounds.

Generally, when looking at dihedral angle distributions, the narrower the torsional range, the smaller the structural fluctuation. Thus, in order to provide a deeper analysis of the fluctuations of our new compounds in complex with 5-HT_{1B}, compared to DHE and ERG, we calculated the dihedral angle distributions (Figure S18-S19). All calculated dihedral angles are shown here, however we chose to focus on the light blue and light green torsional angles, as well as minor interests in the light purple torsional angles, since these were the torsional angles for which our predictions were made. Evident from the original ergotamine light blue torsional angle, the two major angles are around +90 and -90 degrees, however there is a wide distribution overall. Looking at the light blue torsional angles for the ERG compounds, it is evident that this range was significantly decrease to -90 degrees for compound 1 and +90 degrees for compound 2. Similar patterns can be observed for the light green torsional angles where there is a huge distribution in the original ergotamine simulation with major peaks at -180, -90, +90, and +180 degrees. However, in both compounds the distribution is significantly decreased to -90 and +90 degrees for compound 1 and just +90 degrees for compound 2. Although the contrast is not as profound for the light purple torsional angles, both compounds have a slightly more narrow distribution when compared to ergotamine. For the dihydroergotamine compounds, we observe the same pattern where for the light blue and light green torsional angles there is a significant decrease in the distribution of the angles, and a marginal decrease is observed for the light purple angle. Specifically, the original dihydroergotamine ligand shows widespread peaks at both -90 and +90 degrees for the light blue torsional angle. When comparing the light blue torsional angle of the new compounds to DHE both compounds 1 and 2 show the angle shift only to ~-90 degrees and for compound 3 this shift is toward +90 degrees. For the light green angle, DHE shows small peaks ranging from -90 to -180 degrees and a large peak around +90 degrees.

However, this peak is primarily shifted to -180 degrees in compound 1, +90 degrees in compound 2, and although there is still a distribution for compound 3 the shift was primarily toward -90 degrees. For the light purple angle, compounds 1 and 3 show similar patterns with a more narrow distribution, whereas compound 2 has a peak shift to -180 degrees. Overall, these decreased distributions of torsional angles at the specific angles for which our predictions were made provide further support that the compounds selected from our virtual screening would show a decreased structural fluctuation upon binding. Thus suggesting that these compounds would be more stable and bind more favorably to 5-HT_{1B} than ERG or DHE, respectively.

We also analyzed the interactions of each compounds at 5-HT_{1B} which are represented here using a two dimensional ligand interaction diagram for ERG and compounds (Figure S20) as well as DHE and compounds (Figure S21). From these diagrams it is clear that for both the ERG and DHE compounds, a majority of the interactions that either ERG or DHE were involved in were maintained, however many compounds were also involved in new interactions which have likely stabilized them which we observed through the RMSF and dihedral angle distribution, as well as contributed to the increase in binding energy as observed in the MMGBSA analysis. Specifically, both ERG compound 1 and 2 showed additional hydrogen bonding between the nitrogen at the second position (see **Figure 7** for reference to numbering) and Ser212^{5.43} and hydrophobic interactions with Ala216^{5.46} when compared to ERG. Although compound 2 loses the polar interaction with Thr355^{7.38} the energy contribution lost from a lack of this interaction is made up through additional hydrophobic interactions with Phe351^{7.34} and Trp327^{6.48}. On the other hand, the DHE compounds show a little more variation when compared to DHE. Both DHE Compounds 1 and 2 maintained interactions with Asp129^{3.32}, Val201^{ECL2}, and Thr355^{7.38}, and compound 3 maintained interactions with Asp129^{3.32}, Val201^{ECL2} and Cys133^{3,36}. However none of the compounds interacted with Thr134^{3,37}. In terms of new interactions conserved between compounds, compounds 1 and 3 formed hydrophobic

interactions with Ile339^{6.60}, compound 1 and 2 formed polar interactions with Tyr359^{7.42}, and compounds 2 and 3 formed hydrophobic interactions with Cys340^{ECL3}. Interactions unique to compound 2 include hydrogen bonding to Gly113^{2.68}, hydrophobic interactions with Tyr109^{2.64} and Leu126^{3,29}, and negatively charged interactions with Asp352^{7,35}, and compound 3 formed hydrophobic interactions with Ile130^{3.33}. Interestingly, when comparing these results to the MMGBSA, the additional interactions formed between DHE compound 2 and 5-HT_{1B} did not result in the most energetically favorable DHE compound. One possibility is that DHE's interaction plays a significant role in the final binding pose where compound 1 has 5 interactions with water, DHE and compound 3 both have 3 interactions with water, but compound 2 only has two water interactions. On the other hand DHE compound 3 may have a more favorable binding energy due to its unique interactions with Ile130^{3,33}, which is known to contribute to a multiresidue hydrophobic cleft which is known to stabilize the planar ergoline moiety. Nonetheless, by comparing the interactions of each compound at the binding pocket of 5-HT_{1B} to the original ligand, DHE or ERG, we identified potential residues which may have contributed to the observed change in binding energy and the decreased fluctuations that led to an increased stability for each new compound complex.

Conclusion

ERG and DHE differ by only a single π bond, yet have been shown to have almost a ten-fold activity difference at the 5-HT_{1B} receptor. The crystal structures of the 5-HT_{1B} receptor in complex with both ligands have been resolved, but the high similarity between two complexes cannot sufficiently explain their activity difference. Hence, an examination of the dynamic motion of both drugs with the receptor is needed. By comparing the complex trajectories and protein-ligand interactions, a better understanding of the activity differences between the two ligands was

realized. The ligand-protein interactions and secondary structures of the ligands showed subtle variations. More notably, the ligand and protein RMSFs for the systems were distinct, with ERG having a trend of lower RMSF values, indicating it to be more tightly bound to 5-HT_{1B} with less fluctuations. The MM-GBSA binding energies further illustrate this, as ERG has an overall stronger MM-GBSA binding energy by -15 kcal/mol. The difference of active and inactive states at the Tyr toggle switch (NPXXY) may suggest different signal transduction pathways for each ligand. Our dynamic network model and normal mode analysis also show differences in the dynamics of the two complex systems. Using our critical nodes and readily available mutagenesis data, we identify $W327^{6.48}$ and $F331^{6.52}$ as key residues involved in the active state of 5-HT_{1B}. All of which provides dynamic insight into the crystal structures of ergotamine-5-HT_{1B} and dihydroergotamine-5-HT_{1B} receptor complexes. This dynamic insight helps to explain the activity differences of these two molecules which was unclear from the crystal structures. Using the detailed dynamic insights gained from our study we were able to predict potential modification sites of both DHE and ERG which yielded compounds that show more favorable binding energies and reduced structural fluctuation. These derivatives might be good candidates for further experimental tests. Clearly, molecular dynamics can add additional important knowledge that cannot be garnered from structure alone.

Supporting Information

Included in the supporting documents are the receptor sequence, the most abundant receptor-ligand complexes from clustering analysis, superposition of the most abundant conformations from the

MD simulations of the receptor with the ligands, example of a protein-ligand contact table, and the complete set of ligand torsion plots for all rotatable bonds throughout the MD trajectory.

Acknowledgments

This work was supported by Rowan CSM SEED grant and the National Science Foundation under Grants NSF ACI-1429467/RUI-1904797 and XSEDE MCB 170088.

References

- 1. Wermuth, C. G.; Grisoni, S.; Villoutreix, B.; Rocher, J.-P. Chapter 12 Application Strategies for the Primary Structure–Activity Relationship Exploration. In *The Practice of Medicinal Chemistry (Fourth Edition)*; Academic Press: San Diego, 2015, pp 301-318.
- 2. Chan, S. L. F.; Pallett, A. L.; Morgan, N. G., Clotrimazole and Efaroxan Stimulate Insulin Secretion by Different Mechanisms in Rat Pancreatic Islets. *Naunyn-Schmiedeberg's Arch. Pharmacol.* **1997**, 356, 763-768.
- 3. Chan, S. L. F.; Atlas, D.; James, R. F. L.; Morgan, N. G., The Effect of the Putative Endogenous Imidazoline Receptor Ligand, Clonidine-Displacing Substance, on Insulin Secretion from Rat and Human Islets of Langerhans. *Br. J. Pharmacol.* **1997**, 120, 926-932.
- 4. Morgan, N. G.; Chan, S. L. F.; Mourtada, M.; Monks, L. K.; Ramsden, C. A. Imidazolines and Pancreatic Hormone Secretion. In *Imidazoline Receptors and Their Endogenous Ligands: Current Concepts and Therapeutic Potential*, Gothert, M.; Molerings, G. J.; Reis, D. J., Eds.; 1999; Vol. 881, pp 217-228.
- 5. Brown, C. A.; Chan, S. L. F.; Stillings, M. R.; Smith, S. A.; Morgan, N. G., Antagonism of the Stimulatory Effects of Efaroxan and Glibenclamide in Rat Pancreatic Islets by the Imidazoline, RX801080. *Br. J. Pharmacol.* **1993**, 110, 1017-1022.
- 6. Rothlin, E., Historical Development of the Ergot Therapy of Migraine. *Int. Arch. Allergy Immunol.* **1955**, 7, 205-209.
- 7. Silberstein, S. D.; McCrory, D. C., Ergotamine and Dihydroergotamine: History, Pharmacology, and Efficacy. *Headache* **2003**, 43, 144-166.
- 8. Friedman, A. P.; Von Storch, T. J., Recent Advances in Treatment of Migraine. *J. Am. Med. Assoc* **1951**, 145, 1325-8.
- 9. Lipton, R. B., Ergotamine Tartrate and Dihydroergotamine Mesylate: Safety Profiles. *Headache* **1997**, 37, S33-S41.
- 10. Saper, J. R.; Silberstein, S., Pharmacology of Dihydroergotamine and Evidence for Efficacy and Safety in Migraine. *Headache* **2006**, 46, S171-S181.
- 11. Morren, J. A.; Galvez-Jimenez, N., Where is Dihydroergotamine Mesylate in the Changing Landscape of Migraine Therapy? *Expert Opin. Pharmacother.* **2010**, 11, 3085-3093.

- 12. Silberstein, S. D., The Pharmacology of Ergotamine and Dihydroergotamine. *Headache* **1997**, 37, S15-S25.
- 13. Villalon, C. M.; De Vries, P.; Rabelo, G.; Centurion, D.; Sanchez-Lopez, A.; Saxena, P., Canine External Carotid Vasoconstriction to Methysergide, Ergotamine and Dihydroergotamine: Role of 5-HT(1B/1D) Receptors and Alpha(2)-Adrenoceptors. *Br. J. Pharmacol.* **1999**, 126, 585-594.
- 14. Hoyer, D., Functional Correlates of Serotonin 5-HT1 Recognition Sites. *J. Recept. Res.* **1988**, 8, 59-81.
- 15. Leysen, J. E.; Gommeren, W.; Heylen, L.; Luyten, W.; VandeWeyer, I.; Vanhoenacker, P.; Haegeman, G.; Schotte, A.; VanGompel, P.; Wouters, R.; Lesage, A. S., Alniditan, a New 5-hydroxytryptamine(1D) Agonist and Migraine-Abortive Agent: Ligand-Binding Properties of Human 5-Hydroxytryptamine(1D alpha), Human 5-Hydroxytryptamine(1D beta), and Calf 5-Hydroxytryptamine(1D) Receptors Investigated with H-3 5-hydroxytryptamine and H-3 Alniditan. *Mol. Pharmacol.* **1996**, 50, 1567-1580.
- 16. Wang, C.; Jiang, Y.; Ma, J. M.; Wu, H. X.; Wacker, D.; Katritch, V.; Han, G. W.; Liu, W.; Huang, X. P.; Vardy, E.; McCorvy, J. D.; Gao, X.; Zhou, X. E.; Melcher, K.; Zhang, C. H.; Bai, F.; Yang, H. Y.; Yang, L. L.; Jiang, H. L.; Roth, B. L.; Cherezov, V.; Stevens, R. C.; Xu, H. E., Structural Basis for Molecular Recognition at Serotonin Receptors. *Science (New York, N.Y.)* **2013**, 340, 610-614.
- 17. Karplus, M.; McCammon, J. A., Molecular Dynamics Simulations of Biomolecules. *Nat. Struct. Biol.* **2002**, 9, 646-652.
- 18. Vaidehi, N.; Bhattacharya, S.; Larsen, A. B. Structure and Dynamics of G-Protein Coupled Receptors. In *G Protein-Coupled Receptors Modeling and Simulation*, Filizola, M., Ed.; 2014; Vol. 796, pp 37-54.
- 19. Gonzalez, A.; Cordomi, A.; Matsoukas, M.; Zachmann, J.; Pardo, L. Modeling of G Protein-Coupled Receptors Using Crystal Structures: From Monomers to Signaling Complexes. In *G Protein-Coupled Receptors Modeling and Simulation*, Filizola, M., Ed.; 2014; Vol. 796, pp 15-33.
- 20. Chan, H. C. S.; Li, Y.; Dahoun, T.; Vogel, H.; Yuan, S., New Binding Sites, New Opportunities for GPCR Drug Discovery. *Trends Biochem. Sci.* **2019**, 44, 312-330.
- 21. Kakarala, K. K.; Jamil, K.; Devaraji, V., Structure and Putative Signaling Mechanism of Protease Activated Receptor 2 (PAR2) A Promising Target for Breast Cancer. *J. Mol. Graphics Modell.* **2014**, 53, 179-199.
- 22. Costanzi, S.; Skorski, M.; Deplano, A.; Habermehl, B.; Mendoza, M.; Wang, K.; Biederman, M.; Dawson, J.; Gao, J., Homology Modeling of a Class A GPCR in the Inactive Conformation: A Quantitative Analysis of the Correlation Between Model/Template Sequence Identity and Model Accuracy. *J. Mol. Graphics Modell.* **2016**, 70, 140-152.
- 23. Wang, T.; Duan, Y., Ligand Entry and Exit Pathways in the Beta2-Adrenergic Receptor. *Am. J. Mol. Biol.* **2009**, 392, 1102-1115.
- 24. Wang, T.; Duan, Y., Binding Modes of CCR5-targetting HIV Entry Inhibitors: Partial and Full Antagonists. *J. Mol. Graphics Modell.* **2008**, 26, 1287-1295.
- 25. Wang, T.; Duan, Y., Retinal Release from Opsin in Molecular Dynamics Simulations. *J. Mol. Recognit.* **2011**, 24, 350-358.
- 26. Chan, H. C. S.; Wang, J.; Palczewski, K.; Filipek, S.; Vogel, H.; Liu, Z.-J.; Yuan, S., Exploring a New Ligand BInding Site of G Protein-Coupled Receptors. *Chem. Sci.* **2018**, 9, 6480-6489.
- 27. Liu, M.; Wang, L.; Zhao, X.; Sun, X., Molecular Recognition of Agonist and Antagonist for Peroxisome Proliferator-Activated Receptor-α Studied by Molecular Dynamics Simulations. *Int. J. Mol. Sci.* **2014**, 15, 8743-8752.

- 28. Liao, C.; May, V.; Li, J., PAC1 Receptors: Shapeshifters in Motion. *J. Mol. Neurosci.* **2018**, 68, 331-339.
- 29. Lu, S.; Zhang, J., Small Molecule Allosteric Modulators of G-Protein-Coupled Receptors: Drug-Target Interactions. *J. Med. Chem.* **2018**, 62, 24-45.
- 30. Lu, S.; Shen, Q.; Zhang, J., Allosteric Methods and Their Applications: Facilitating the Discovery of Allosteric Drugs and the Investigation of Allosteric Mechanisms. *Acc. Chem. Res.* **2019**, 52, 492-500.
- 31. Ni, D.; Chen, G.; Song, K.; Huang, M.; Lu, S.; Liu, X.; Shen, Q.; Zhang, J.; Gao, J.; Li, Q.; Hong, Y.; Wang, R.; Xu, J., AlloFinder: A Strategy for Allosteric Modulator Discovery and Allosterome Analyses. *Nucleic Acids Res.* **2018**, 46, W451-W458.
- 32. Zhang, F.; Yuan, Y.; Xiang, M.; Guo, Y.; Li, M.; Liu, Y.; Pu, X., Molecular Mechanism Regarding Allosteric Modulation of Ligand Binding and the Impact of Mutations on Dimerization for CCR5 Homodimer. *J. Chem. Inf. Model.* **2019**, 59, 1965-1976.
- 33. Wang, L. R.; Yuan, Y.; Chen, X.; Chen, J. F.; Guo, Y. Z.; Li, M. L.; Li, C.; Pu, X. M., Probing the Cooperative Mechanism of The Opioid Receptor Heterodimer by Multiscale Simulation. *Phys. Chem. Chem. Phys.* **2018**, 20, 29969-29982.
- 34. Montgomery, D.; Campbell, A.; Sullivan, H.-J.; Wu, C., Molecular Dynamics Simulation of Biased Agonists at the Dopamine D2 Receptor Suggests the Mechanism of Receptor Functional Selectivity. *J. Biomol. Struct. Dyn.* **2019**, 37, 3206-3225.
- 35. Sader, S.; Anant, K.; Wu, C., To Probe Interaction of Morphine and IBNtxA with 7TM and 6TM Variants of the Human μ -Opioid Receptor Using All-Atom Molecular Dynamics Simulations with an Explicit Membrane. *Phys. Chem. Phys.* **2018**, 20, 1724-1741.
- 36. Sader, S.; Cai, J.; Muller, A. C. G.; Wu, C., Can Human Allergy Drug Fexofenadine, an Antagonist of Histamine (H(1)) Receptor, Be Used to Treat Dog and Cat? Homology Modeling, Docking and Molecular Dynamic Simulation of Three H(1) Receptors in Complex with Fexofenadine. *J. Mol. Graphics Modell.* **2017**, 75, 106-116.
- 37. Sylte, I.; Edvardsen, O.; Dahl, S. G., Molecular Dynamics of the 5-HT1a Receptor and Ligands. *Protein Eng.* **1993**, 6, 691-700.
- 38. Sylte, I.; Bronowska, A.; Dahl, S. G., Ligand Induced Conformational States of the 5-HT1A Receptor. *Eur. J. Pharmacol.* **2001**, 416, 33-41.
- 39. Seeber, M.; De Benedetti, P. G.; Fanelli, F., Molecular Dynamics Simulations of the Ligand-Induced Chemical Information Transfer in the 5-HT1A Receptor. *J. Chem. Inf. Model.* **2003**, 43, 1520-1531.
- 40. Marti-Solano, M.; Sanz, F.; Pastor, M.; Selent, J., A Dynamic View of Molecular Switch Behavior at Serotonin Receptors: Implications for Functional Selectivity. *PloS one* **2014**, 9.
- 41. Bowerman, S.; Wereszczynski, J., Detecting Allosteric Networks Using Molecular Dynamics Simulation. *Methods Enzymol* **2016**, 578, 429-447.
- 42. Stolzenberg, S.; Michino, M.; LeVine, M. V.; Weinstein, H.; Shi, L., Computational Approaches to Detect Allosteric Pathways in Transmembrane Molecular Machines. *Biochim. Biophys. Acta, Biomembr.* **2016**, 1858, 1652-1662.
- 43. La Sala, G.; Decherchi, S.; De Vivo, M.; Rocchia, W., Allosteric Communication Networks in Proteins Revealed through Pocket Crosstalk Analysis. *ACS Cent Sci* **2017**, 3, 949-960.
- 44. Mishra, S. K.; Jernigan, R. L., Protein Dynamic Communities From Elastic Network Models Align Closely to the Communities Defined by Molecular Dynamics. *PloS one* **2018**, 13, e0199225.
- 45. Schneider, S.; Provasi, D.; Filizola, M., How Oliceridine (TRV-130) Binds and Stabilizes a μ-Opioid Receptor Conformational State That Selectively Triggers G Protein Signaling Pathways. *Biochemistry* **2016**, 55, 6456-6466.

- 46. Jiang, Y.; Yuan, Y.; Zhang, X.; Liang, T.; Guo, Y.; Li, M.; Pu, X., Use of Network Model to Explore Dynamic and Allosteric Properties of Three GPCR Homodimers. *RSC Adv.* **2016**, 6, 106327-106339.
- 47. Sastry, G. M.; Adzhigirey, M.; Day, T.; Annabhimoju, R.; Sherman, W., Protein and Ligand Preparation: Parameters, Protocols, and Influence on Virtual Screening Enrichments. *J. Comput.-Aided Mol. Des.* **2013**, 27, 221-234.
- 48. Lyman, E.; Higgs, C.; Kim, B.; Lupyan, D.; Shelleys, J. C.; Farid, R.; Voth, G. A., A Role for a Specific Cholesterol Interaction in Stabilizing the Apo Configuration of the Human A(2A) Adenosine Receptor. *Structure* **2009**, 17, 1660-1668.
- 49. Mark, P.; Nilsson, L., Structure and Dynamics of the TIP3P, SPC, and SPC/E Water Models at 298 K. *J. Phys. Chem. A* **2001**, 105, 9954-9960.
- 50. Wang, M.; Xie, W.; Li, A.; Xu, S., Structural Basis and Mechanism of Chiral Benzedrine Molecules Interacting With Third Dopamine Receptor. *Chirality* **2016**, 28, 674-685.
- 51. Harder, E.; Damm, W.; Maple, J.; Wu, C. J.; Reboul, M.; Xiang, J. Y.; Wang, L. L.; Lupyan, D.; Dahlgren, M. K.; Knight, J. L.; Kaus, J. W.; Cerutti, D. S.; Krilov, G.; Jorgensen, W. L.; Abel, R.; Friesner, R. A., OPLS3: A Force Field Providing Broad Coverage of Drug-like Small Molecules and Proteins. *J. Chem. Theory Comput.* **2016**, 12, 281-296.
- 52. Zhang, J.; Hou, Y.; Wang, Y.; Wang, C.; Zhang, X., The LBFGS quasi-Newtonian method for molecular modeling prion AGAAAAGA amyloid fibrils. *Natural Science* **2012**, 04, 1097-1108.
- 53. Ikeguchi, M., Partial Rigid-Body Dynamics in NPT, NPAT and NPgammaT Ensembles for Proteins and Membranes. *J Comput Chem* **2004**, 25, 529-541.
- 54. Bailey, A. G.; Lowe, C. P., MILCH SHAKE: An Efficient Method for Constraint Dynamics Applied to Alkanes. *J Comput Chem* **2009**, 30, 2485-2493.
- 55. Shan, Y.; Klepeis, J. L.; Eastwood, M. P.; Dror, R. O.; Shaw, D. E., Gaussian Split Ewald: A Fast Ewald Mesh Method for Molecular Simulation. *J. Chem. Phys.* **2005**, 122, 54101-54101.
- 56. Stuart, S. J.; Zhou, R.; Berne, B. J., Molecular Dynamics with Multiple Time Scales: The Selection of Efficient Reference System Propagators. *J. Chem. Phys.* **1996**, 105, 1426-1436.
- 57. Bowers, K. J.; Chow, E.; Xu, H.; Dror, R. O.; Eastwood, M. P.; Gregersen, B. A.; Klepeis, J. L.; Kolossvary, I.; Moraes, M. A.; Sacerdoti, F. D.; Salmon, J. K.; Shan, Y.; Shaw, D. E., In *Proceedings of the 2006 ACM/IEEE conference on Supercomputing*; ACM: Tampa, Florida, 2006, p 84.
- 58. Hou, T. J.; Wang, J. M.; Li, Y. Y.; Wang, W., Assessing the Performance of the MM/PBSA and MM/GBSA Methods. 1. The Accuracy of Binding Free Energy Calculations Based on Molecular Dynamics Simulations. *J. Chem. Inf. Model.* **2011**, 51, 69-82.
- 59. Xu, L.; Sun, H. Y.; Li, Y. Y.; Wang, J. M.; Hou, T. J., Assessing the Performance of MM/PBSA and MM/GBSA Methods. 3. The Impact of Force Fields and Ligand Charge Models. *J. Phys. Chem. B* **2013**, 117, 8408-8421.
- 60. Sun, H. Y.; Li, Y. Y.; Tian, S.; Xu, L.; Hou, T. J., Assessing the Performance of MM/PBSA and MM/GBSA Methods. 4. Accuracies of MM/PBSA and MM/GBSA Methodologies Evaluated by Various Simulation Protocols Using PDBbind Data Set. *Phys. Chem. Chem. Phys.* **2014**, 16, 16719-16729.
- 61. Li, J.; Abel, R.; Zhu, K.; Cao, Y.; Zhao, S.; Friesner, R. A., The VSGB 2.0 model: A next generation energy model for high resolution protein structure modeling. *Proteins: Structure, Function, and Bioinformatics* **2011**, 79, 2794-2812.
- 62. Ghosh, A.; Rapp, C. S.; Friesner, R. A., Generalized Born Model Based on a Surface Integral Formulation. *J. Phys. Chem. B* **1998**, 102, 10983-10990.

- 63. Kollman, P.; Massova, I.; Reyes, C.; Kuhn, B.; Huo, S.; Chong, L.; Lee, M.; Lee, T.; Duan, Y.; Wang, W.; Donini, O.; Cieplak, P.; Srinivasan, J.; Case, D.; Cheatham, T., Calculating Structures and Free Energies of Complex Molecules: Combining Molecular Mechanics and Continuum Models. *Acc. Chem. Res.* **2000**, 33, 889-897.
- 64. Hou, T.; Wang, J.; Li, Y.; Wang, W., Assessing the Performance of the Molecular Mechanics/Poisson Boltzmann Surface Area and Molecular Mechanics/Generalized Born Surface Area Methods. II. The Accuracy of Ranking Poses Generated from Docking. *J. Comput. Chem.* **2010**, 32, 866-877.
- 65. Eargle, J.; Luthey-Schulten, Z., NetworkView: 3D Display and Analysis of Protein RNA Interaction Networks. *Bioinformatics* **2012**, 28, 3000-3001.
- 66. del Sol, A.; Fujihashi, H.; Amoros, D.; Nussinov, R., Residues Crucial for Maintaining Short Paths in Network Communication Mediate Signaling in Proteins. *Mol. Syst. Biol.* **2006**, 2, 2006.0019-2006.0019.
- 67. Ghosh, A.; Vishveshwara, S., A Study of Communication Pathways in Methionyl- tRNA Synthetase by Molecular Dynamics Simulations and Structure Network Analysis. *Proc. Natl. Acad. Sci. U. S. A.* **2007**, 104, 15711-15716.
- 68. Chennubhotla, C.; Bahar, I., Markov Propagation of Allosteric Effects in Biomolecular Systems: Application to GroEL–GroES. *Mol. Syst. Biol.* **2006**, 2, 36.
- 69. Sethi, A.; Eargle, J.; Black, A. A.; Luthey-Schulten, Z., Dynamical Networks in tRNA:Protein Complexes. *Proc. Natl. Acad. Sci.* **2009**, 106, 6620.
- 70. Humphrey, W., Dalke, A. and Schulten, K, "VMD Visual Molecular Dynamics". *J. Molec. Graphics* **1996**, 14, 33-38.
- 71. Glykos, N. M., Software News and Updates. Carma: A Molecular Dynamics Analysis Program. *J Comput Chem* **2006**, 27, 1765-1768.
- 72. Bhattacharyya, M.; Bhat, C. R.; Vishveshwara, S., An Automated Approach to Network Features of Protein Structure Ensembles. *Protein Sci.* **2013**, 22, 1399-1416.
- 73. Gadiyaram, V.; Vishveshwara, S.; Vishveshwara, S., From Quantum Chemistry to Networks in Biology: A Graph Spectral Approach to Protein Structure Analyses. *J. Chem. Inf. Model.* **2019**, 59, 1715-1727.
- 74. Girvan, M.; Newman, M. E. J., Community Structure in Social and Biological Networks. *Proc. Natl. Acad. Sci.* **2002**, 99, 7821.
- 75. Bakan, A.; Meireles, L. M.; Bahar, I., ProDy: Protein Dynamics Inferred from Theory and Experiments. *Bioinformatics* **2011**, 27, 1575-1577.
- 76. Friesner, R. A.; Banks, J. L.; Murphy, R. B.; Halgren, T. A.; Klicic, J. J.; Mainz, D. T.; Repasky, M. P.; Knoll, E. H.; Shelley, M.; Perry, J. K.; Shaw, D. E.; Francis, P.; Shenkin, P. S., Glide: A New Approach for Rapid, Accurate Docking and Scoring. 1. Method and Assessment of Docking Accuracy. *J. Med. Chem.* **2004**, 47, 1739-1749.
- 77. Ioakimidis, L.; Thoukydidis, L.; Mirza, A.; Naeem, S.; Reynisson, J., Benchmarking the Reliability of QikProp. Correlation Between Experimental and Predicted Values. *QSAR Comb. Sci.* **2008**, 27, 445-456.
- 78. Ballesteros, J. A.; Weinstein, H. [19] Integrated Methods for the Construction of Three-Dimensional Models and Computational Probing of Structure-Function Relations in G Protein-Coupled Receptors. In *Methods in Neurosciences*, Sealfon, S. C., Ed.; Academic Press: 1995; Vol. 25, pp 366-428.
- 79. Trzaskowski, B.; Latek, D.; Yuan, S.; Ghoshdastider, U.; Debinski, A.; Filipek, S., Action of Molecular Switches in GPCRs--Theoretical and Experimental Studies. *Curr. Med. Chem.* **2012**, 19, 1090-1109.
- 80. Yin, W.; Zhou, X. E.; Yang, D.; de Waal, P. W.; Wang, M.; Dai, A.; Cai, X.; Huang, C.-Y.; Liu, P.; Wang, X.; Yin, Y.; Liu, B.; Zhou, Y.; Wang, J.; Liu, H.; Caffrey, M.; Melcher, K.;

- Xu, Y.; Wang, M.-W.; Xu, H. E.; Jiang, Y., Crystal Structure of the Human 5-HT(1B) Serotonin Receptor Bound to an Inverse Agonist. *Cell Discov* **2018**, 4, 12-12.
- 81. Vass, M.; Podlewska, S.; de Esch, I. J. P.; Bojarski, A. J.; Leurs, R.; Kooistra, A. J.; de Graaf, C., Aminergic GPCR–Ligand Interactions: A Chemical and Structural Map of Receptor Mutation Data. *J. Med. Chem.* **2019**, 62, 3784-3839.
- 82. Granas, C.; Nordquist, J.; Mohell, N.; Larhammar, D., Site-Directed Mutagenesis of the 5-HT1B Receptor Increases the Affinity of 5-HT for the Agonist Low-Affinity Conformation and Reduces the Intrinsic Activity of 5-HT. *Eur. J. Pharmacol.* **2001**, 421, 69-76.
- 83. Nair, P. C.; Miners, J. O., Molecular Dynamics Simulations: From Structure Function Relationships to Drug Discovery. *In Silico Pharmacol.* **2014**, 2, 4.

Table of Contents graphics

